Anton Paar

Building Materials

E-Book

Building Better: Practical Guides for Great Building Materials

The building materials and construction industry is evolving rapidly to meet demands for sustainability, resilience, and efficiency. Trends such as using recycled materials, 3D printing, carbon-neutral construction, and resource optimization are transforming material design and application to address environmental and performance challenges.

This e-book provides a concise guide to analyzing and optimizing building materials, covering cement, concrete, metals, composites, and architectural finishes. With real-world case studies and practical insights, this resource supports professionals in research, quality assurance, and engineering, equipping them to improve material performance and address industry challenges effectively.

1 Analytical Methods to Characterize Cement

Cement is one of the most essential building materials, forming the backbone of modern construction. From residential homes to large-scale infrastructure projects, cement is used to bind materials together, ensuring structural integrity and durability. Understanding the physical and chemical properties of cement is critical for optimizing its production, application, and performance in various environmental conditions. The quality and efficiency of cement production depend on precise control over several parameters, including particle size and shape, chemical composition, and rheological properties. These factors directly influence key characteristics such as setting time, strength, and durability.

In this chapter, we delve into the analytical methods and technologies used to study cement's properties. From particle size distribution to setting behavior, from moisture analysis to mechanical properties, each section provides insights into how these measurements drive improvements in cement production and application. By leveraging these advanced techniques, manufacturers can ensure consistent product quality, meet environmental regulations, and enhance material performance in demanding applications.

1.1 PARTICLE SIZE AND SHAPE ANALYSIS OF CEMENT

Grinding is an energy-intensive process, making efficient parameter management economically crucial. Narrowing the particle size distribution (PSD) typically reduces energy and costs. However, the grindability of cement components varies, with softer materials having broader PSDs. Paradoxically, adding softer components (broader PSD) narrows the PSD of harder components, and vice versa[1]. Since grinding is strongly influenced by PSD, its analysis is integral at nearly every production stage.

Particle size also significantly impacts the final product's properties. Alongside clinker composition and specific surface area, PSD is a key factor shaping the hydration curve and strength of hardened cement[2]. Smaller particle sizes accelerate setting and enhance early strength, while coarser particles gain importance as cement ages[2][3]. Additionally, PSD width affects water demand[1]. In summary, adjusting particle size and distribution allows for tailoring cement properties.

	LIQUID DISPERSION	DRY DISPERSION
D_{10}	2.97 µm	1.85 µm
D_{50}	15.33 µm	16.20 µm
D_{90}	42.79 µm	49.40 µm

Table 1: Comparison of the results for particle size distribution of cement obtained by liquid and dry measurement.

Measuring PSD in cement is challenging due to its broad size range (sub-micron to over 100 µm), irregular particle shapes, and tendency to agglomerate in the dry state, requiring proper dispersion. The results demonstrate the accuracy of dry cement PSD analysis using a laser diffraction particle size analyzer with dry jet dispersion. Results were compared to measurements in liquid mode using a non-aqueous cement suspension.

The dry and liquid dispersion measurements showed excellent correlation (see Table 1, Figure 1 and Figure 2), confirming that dry dispersion gives accurate PSD measurements.

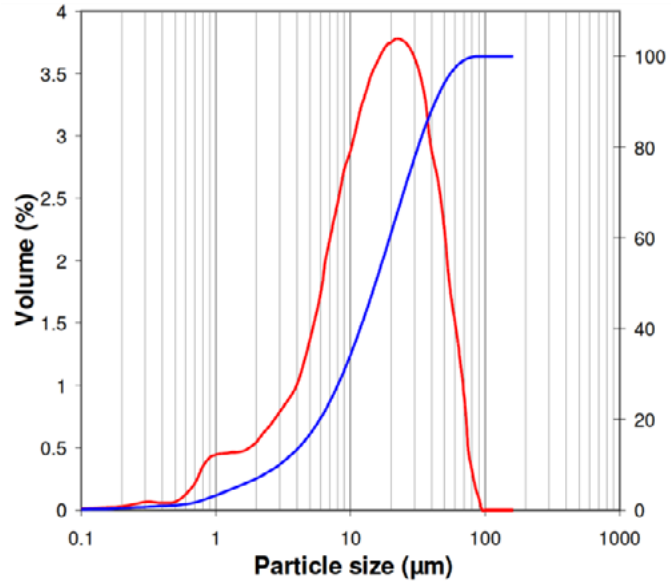

Figure 1: Particle size distribution of cement as measured in liquid mode (ethanol dispersion). Red curve: density distribution (left y-axis); blue curve: cumulative values (right y-axis).

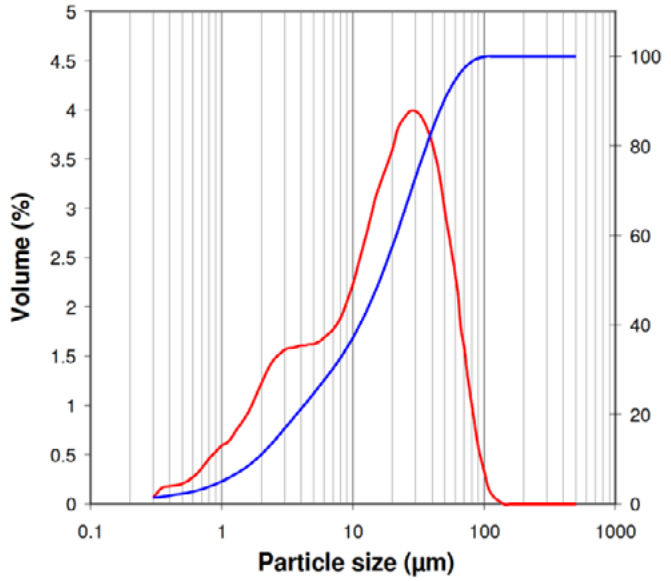

Figure 2: Particle size distribution of cement as measured in dry mode. Red curve: density distribution (left y-axis); blue curve: cumulative values (right y-axis).

In spite of the cohesive properties of cement powder, the dry jet efficiently disperses cement particles at low pressure (less than 1 bar), which prevents possible particle erosion.

INSTRUMENTS SUITABLE FOR THESE MEASUREMENTS
Litesizer DIF 500

To obtain a more comprehensive understanding of cement particles, an additional shape analysis can be conducted using dynamic image analysis. Dynamic image analysis not only gives you the particle size and size distribution but also various shape parameters.

The shape of cement particles is critical in determining the material's performance. Irregular shapes affect cement's handling and mixing characteristics. Optimizing the shape parameters ensures consistent quality, efficient use of materials, and predictable cement performance.

The aspect ratio, a key shape parameter, relates to the minimum and maximum Feret diameters and ranges from 0 (irregular particles) to 1 (perfect spheres). Additional shape parameters, such as ellipse ratio and compactness, may be selected based on particle characteristics and application needs.

While particle size and distribution are standard quality control metrics in cement production, dynamic image analysis enables shape study as an additional control tool, as demonstrated by aspect ratio results in Table 2.

All samples had aspect ratios predominantly between 0.5 and 0.9. Quick-setting cement A3 exhibited the largest, most spherical particles, cement A2 had the smallest particles in a narrower range. These variations are valuable for predicting cement's water demand and performance.

SAMPLES	Q_{10}	Q_{50}	Q90
Cement A1	0.565 ± 0.003	0.746 ± 0.004	0.875 ± 0.001
Cement A2	0.606 ± 0.008	0.775 ± 0.007	0.890 ± 0.004
Cement A3	0.609 ± 0.009	0.775 ± 0.007	0.895 ± 0.003
Cement B1	0.551 ± 0.010	0.745 ± 0.005	0.877 ± 0.002
Cement C1	0.579 ± 0.024	0.763 ± 0.015	0.885 ± 0.003

Table 2: Average and shape (volume-weighted, aspect ratio) results for the measured cement samples.

INSTRUMENTS SUITABLE FOR THESE MEASUREMENTS
Litesizer DIA series

1.2 ACCURATE IDENTIFICATION OF PHASE COMPOSITION WITH X-RAY POWDER DIFFRACTION

X-ray diffraction (XRD) is considered one of the most important analytical methods utilized today to identify and quantify mineral phases in cement and concrete mixtures. This characterization is of particular significance due to the complexity of the composition and interactions between the many polycrystalline minerals found in the material. XRD is able to provide information about the microstructure and characteristic crystalline phases that originate from the clinker and cement manufacturing processes.

Quantifying the amorphous (non-crystalline) and crystalline phases in cementitious materials is essential to understanding and predicting the material's performance and durability during the hydration process. Crystalline phases determine the stability and mechanical properties of the final structure. Amorphous phases contribute to the chemical reactivity, particularly in hydration processes, which directly affects the setting time and strength development of cement. By accurately assessing the balance between these phases, manufacturers can optimize and control cement formulations to achieve desired characteristics.

In this analysis a standard reference Portland cement sample (SRM 2688) from the National Institute of Standards and Technology (NIST) was analyzed under ambient conditions. Typically, cement comprises clinker, gypsum, and in the case of blends, varying concentrations of additives such as fly-ash, and blast furnace slag. For Portland cement specifically, clinker makes up about 95 % of its chemical composition in the form of calcium oxide, silica, alumina, and iron oxide. These four components occur as alite and belite (CaO/SiO_2 compounds), aluminate (CaO/Al_2O_3), and ferrite ($CaO/Al_2O_3/Fe_2O_3$) within the clinker and were therefore the main focus of this investigation.

Qualitative analysis of the measured data allowed easy identification of these four major compounds found in the Portland clinker as seen in Figure 3. A clear distinction between the peaks could be observed over the measured 2θ range.

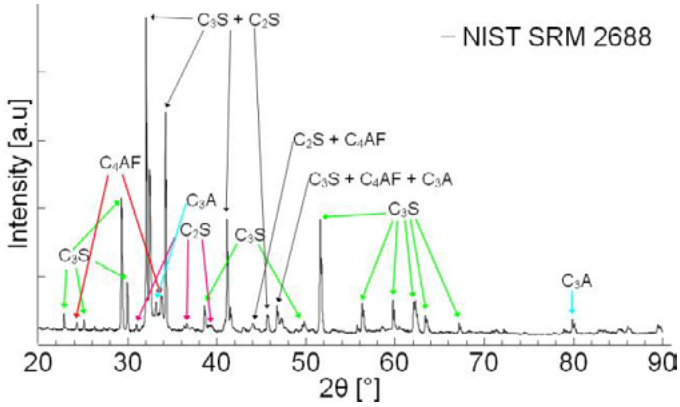

Figure 3: Identification of the crystalline phases in Portland cement clinker. Peaks from the major phases alite (C_3S), belite (C_2S), aluminates (C_3A) and ferrite (C_4AF) are highlighted.

Following identification of the four major phases present in the Portland cement clinker, Rietveld refinement was used to calculate the corresponding phase concentrations. Table 3 compares the mass fractions obtained from the Rietveld refinement of the XRD data to the values from the Certificate of Analysis (CoA) for NIST SRM 2688. Knowledge of the mass fractions is necessary to validate the correct composition of the cement, which defines the material characteristics. In particular the ratio of alite, responsible for early strength development, and belite, which contributes to long-term strength, is a key performance parameter.

PHASE	CoA [wt%]	RESULT [wt%]
Alite	66.1 ± 3.4	67.1
Belite	17.9 ± 3.7	17.0
Ferrite	11.1 ± 5.1	10.3
Aluminate	5.0 ± 2.9	5.6

Table 3: Mass fractions of the four major phases in Portland cement clinker as obtained from the Rietveld analysis of the XRD data and from the Certificate of Analysis (CoA) by liquid and dry measurement.

Based on the results, the mass fractions calculated for the four major phases all fall within the expanded uncertainty (95 % CL) provided by the CoA and thus provide excellent accuracy even for a complex material like cement clinker.

INSTRUMENTS SUITABLE FOR THESE MEASUREMENTS
XRDynamic 500

1.3 MICROWAVE DIGESTION FOR CEMENT INDUSTRY SAMPLES

Trace elements, when introduced into the cement production process, can influence the material's performance, environmental compliance, and structural integrity. The list includes heavy metals, zinc, alkalis, chlorides, and others. Foreign elements can be brought in when using auxiliary or secondary fuels in the rotary kiln. Certainly, the presence of unwanted residues needs to be excluded by careful analysis of the raw materials and fuels used.

Microwave digestion facilitates the ICP analysis of cement-related materials like limestone, clay, marl, secondary fuels, fly ashes, and final products, ensuring effective digestion of complex samples. This analysis supports compliance with environmental regulations and improves process quality.

The digestions for the analysis below were carried out with the Multiwave 5001 microwave digestion platform with the rotor 16HF100 (100 mL PTFE-TFM liner with ceramic pressure jacket, 40 bar, 240 °C), for most of the samples in less than one hour, including the complexation step. The analysis was performed by ICP-OES. Samples included used tyres, fluidized bed combustion ash, plastic scrap, blast furnace slag, marl, and clinker.

SAMPLE	DECOMPOSITION	COMPLEXATION
Used tyres	4 mL HNO_3 2 mL H_2SO_4 0.5 mL HF	3 mL sat. boric acid
Fluidized bed combustion ash	4 mL HNO_3 1 mL HCl 1 mL HF	6 mL sat. boric acid
Plastic scrap	6 mL HNO_3 1 mL HF 0.5 mL HCl	6 mL sat. boric acid
Blast furnace slag, marl	5 mL HNO_3 1 mL HF	6 mL sat. boric acid
Clinker	5 mL HNO_3 1 mL HCl 0.5 mL HF	3 mL sat. boric acid

Table 4: Samples and applied reagents.

All samples were transformed into clear solutions after complexation. The analytical results are displayed in Table 5.

INSTRUMENTS SUITABLE FOR THESE MEASUREMENTS
Multiwave 5001
Multiwave 7101 / 7301 / 7501

ELEMENT	USED TYRES	FL. BED COMB. ASH	PLASTIC SCRAP	BLAST FURNACE SLAG	MARL	CLINKER
As	3.2	5.4		10.8	12.7	8.6
Cd	2.8	4.1	21.1	2.5	3.6	1.9
Cr	7.4	63.6	82.4	30.6	41.2	41.5
Ni	3.2	68.0		3.3	28.6	39.8
Pb	4.8	87.0	133.8	< 0.02	15.1	19.8
Ti	0.4	0.7		1.8	2.3	1.0
V	1.8	43.1		35.8	36.8	37.4
Zn	10400.0	5780.0		255.0	180.0	36.1

Table 5: Analytical results [mg/kg].

1.4 RHEOLOGICAL ANALYSIS OF CEMENT FILLERS

Rheological testing is critical for understanding the flow and setting behavior of cement fillers, essential for ensuring smooth application and surface finishing. The following study evaluated the viscosity, elasticity, and setting characteristics of samples with added modified cement fillers.

Viscosity behavior: As Figure 4 shows, all samples exhibited shear-thinning behavior, where viscosity decreased with increasing shear rate, facilitating smoother application. Sample 1 had the highest viscosity, while Sample 3 had the lowest, making it more prone to sagging during use.

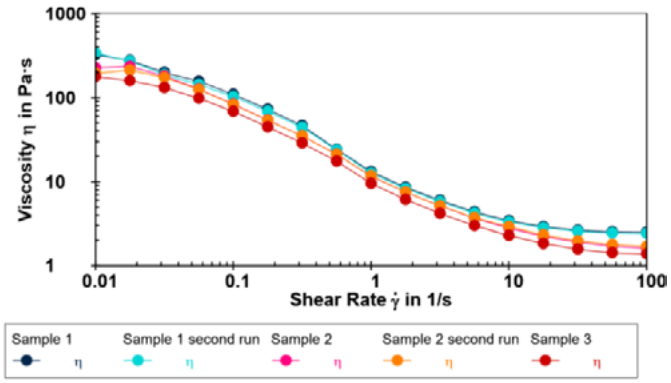

Figure 4: Viscosity curves of all samples.

Elastic properties (Figures 5 and 6): Amplitude sweeps revealed a viscoelastic solid behavior, with elastic modulus (G') values sufficient to maintain form stability in thin layers.

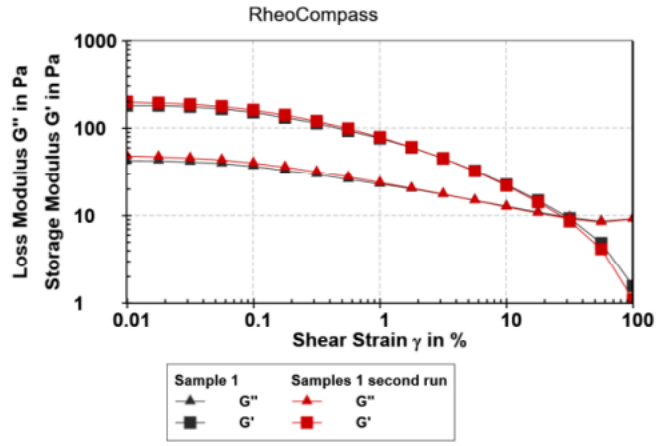

Figure 5: Amplitude sweep (G',G" vs. shear strain) of Sample 1 (repeatability).

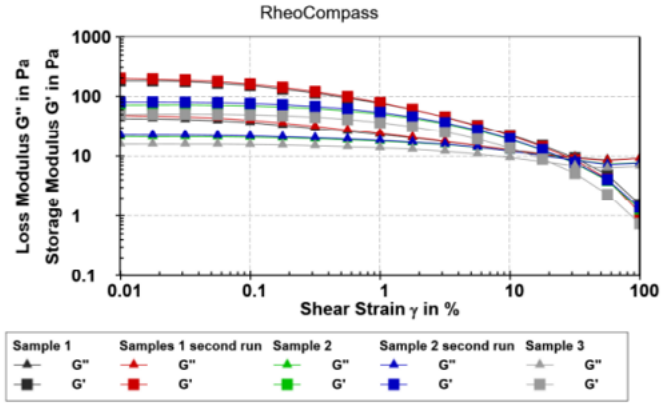

Figure 6: Amplitude sweeps (G',G" vs. shear strain) of all samples.

The crossover point of G' and G" (Table 6) indicated the low stress required for flow initiation, beneficial for application but potentially leading to sagging.

SAMPLE	CROSSOVER POINT G'/G"
Sample 1	4.1 Pa
Sample 2	3.8 Pa
Sample 3	2.3 Pa

Table 6: Crossover points G'/G".

Setting behavior: As illustrated in Figure 7, time-dependent oscillatory tests showed a clear progression in stiffness (G') and energy dissipation (G") during curing. The onset of the chemical reaction (Onset G') occurred after 41.4 minutes for Sample 1, with the reaction rate peaking shortly after. Pot life was determined to be 12.2 minutes for this sample (Table 7).

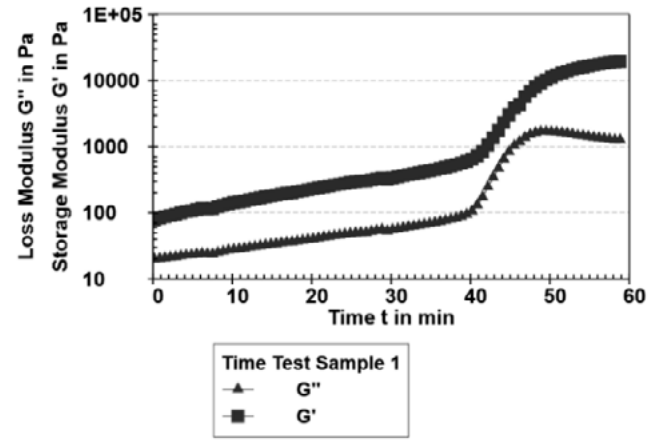

Figure 7: Time-dependent setting of Sample 1.

SAMPLE 1	ONSET G'	INFLECTION G'	MAXIMUM G"	POT LIFE 2 x G'[t0]
Time	41.4 min	44.1 min	50 min	12.2 min

Table 7: Analyzed reaction times of Sample 1.

INSTRUMENTS SUITABLE FOR THESE MEASUREMENTS
MCR Evolution Series with building material cell

1.5 SELECTION OF THE APPROPRIATE CEMENT ADDITIVES FOR COST-REDUCTION WHILE MAINTAINING PRODUCT QUALITY

The cost of construction materials largely depends on the additives used. Research labs often aim to replace costly additives with cheaper alternatives while maintaining material properties. This study examines the impact of methylcellulose I and II on the flow behavior of lime cement plaster and identifies optimal mixing ratios to preserve plaster properties.

Figure 8 shows the flow curves of lime cement plaster (LCP) with varying methylcellulose proportions. Currently, methylcellulose II is used, but replacing it with methylcellulose I is preferable.

Methylcellulose I exhibits similar flow behavior to II but with significantly lower shear stress (around 50 % less). A 50:50 mix closely matches the flow curve of methylcellulose II, with only slight deviations, maintaining similar overall behavior.

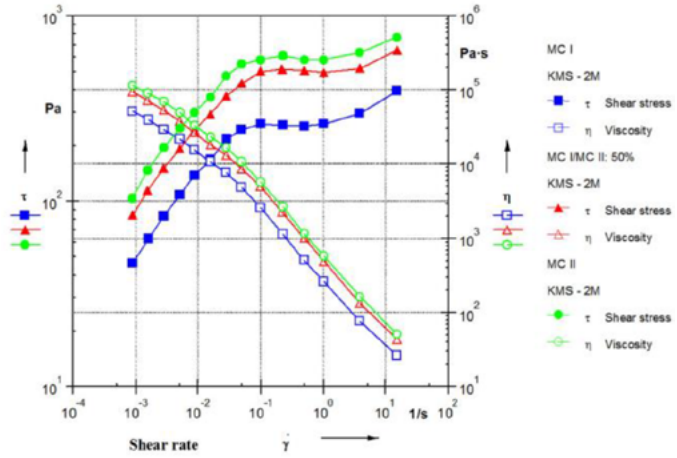

Figure 8: The influence of various methylcellulose mixtures on the flow behavior of a lime cement plaster.

These results highlight methylcellulose II's stronger influence on flow behavior and suggest that a cost-effective 50:50 blend can achieve the desired properties with minimal changes, enabling lower production costs.

INSTRUMENTS SUITABLE FOR THESE MEASUREMENTS
MCR Evolution Series with ball measuring system

1.6 SIMULATION OF DIFFERENT STIRRING METHODS FOR CORRECT USE OF CEMENT COMPOSITION

This chapter illustrates the evaluation of stirring methods to determine which best replicates on-site practices in the laboratory:

→ DIN process (using a Kitchen Aid stirrer)

→ Hand stirring method

Flow behavior was analyzed to assess the suitability of each method, ensuring laboratory preparation mirrors on-site procedures and simulates shear loads. Both methods were compared to the standard on-site stirring process.

Figure 9 shows the flow curves for each method. The DIN method produces lower flow values, reflecting excessive stress on the lime cement plaster (LCP), resulting in overly liquid plaster. This limits its applicability to on-site conditions.

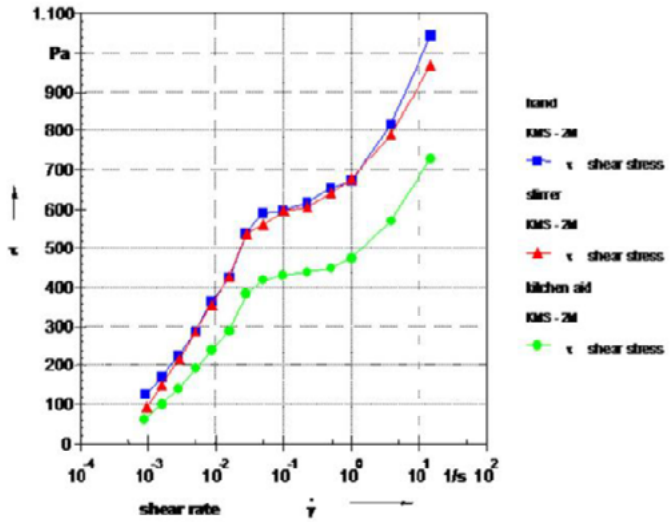

Figure 9: Comparison of flow curves for lime cement plaster prepared using three different stirring methods: Hand-stirred, method used on-site, and a DIN process (Kitchen-Aid).

In contrast, the hand-stirring method closely matches the on-site flow curve across most stress areas. This ensures laboratory results are transferable to field conditions, reducing the need for on-site testing and cutting both time and costs.

INSTRUMENTS SUITABLE FOR THESE MEASUREMENTS

MCR Evolution Series with ball measuring system

1.7 CHARACTERIZATION OF CEMENT AND FLY ASH TO DETERMINE THE CORRECT COMPOSITION

Understanding the rheological properties of cement and fly ash is crucial for optimizing construction materials such as concrete and mortar. These properties directly affect flowability, cohesion, and overall performance, making precise measurements essential for ensuring consistent quality and efficient material use. Fly ash, a byproduct of combustion processes, significantly enhances cement flowability through the "ball bearing effect," where its spherical particles facilitate the sliding of cement particles. Accurate testing methods allow for detecting changes in material mixtures and determining component proportions, which are key for producing cost-effective and reliable construction materials.

The results of the penetration measurements, shown in Figure 10, reveal that Portland cement required the highest penetration force at 4.2 N, signifying strong cohesion, while fly ash showed the lowest force at 2.2 N, reflecting its smoother flow characteristics. The 50:50 mixture of cement and fly ash demonstrated intermediate values, offering a balance of strength and improved flowability.

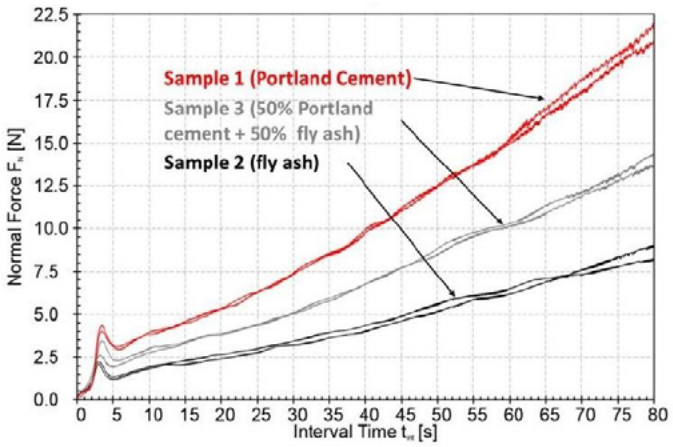

Figure 10: Results of the penetration measurement.

Warren Spring cohesion measurements, illustrated in Figure 11, reinforced these findings, with cement achieving the highest cohesion at 3.37 ± 0.13 kPa and fly ash the lowest at 1.14 ± 0.09 kPa. The mixture displayed moderate cohesion at 2.32 ± 0.10 kPa, striking a balance between ease of handling and structural stability. Adding fly ash to cement liquefies the mixture, enhancing flowability and reducing particle friction, which improves workability and lowers water requirements.

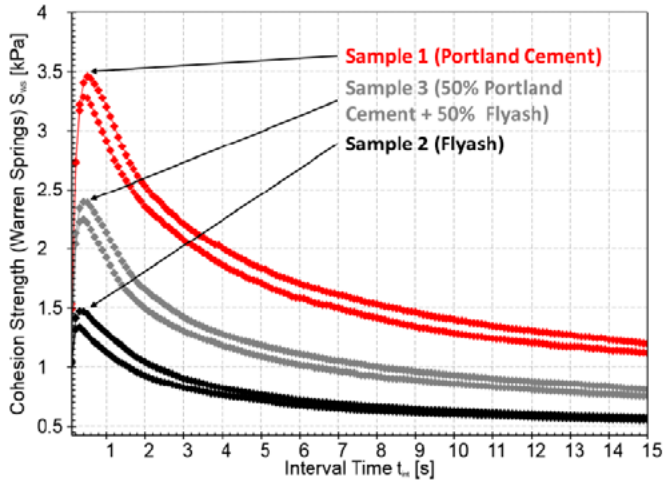

Figure 11: Results of the Warren Spring cohesion measurement.

These results, supported by Figure 10 and Figure 11, highlight the importance of rheological testing in understanding the individual and combined effects of cement and fly ash on material behavior. Such analysis enables manufacturers to fine-tune formulations to meet specific requirements, ensuring optimal performance and reducing costs, thereby enhancing both material efficiency and construction quality.

INSTRUMENTS SUITABLE FOR THESE MEASUREMENTS

MCR Evolution Series with powder flow cell

1.8 HARDNESS TESTING TO INVESTIGATE THE MECHANICAL PROPERTIES OF CEMENT

This chapter demonstrates how the use of advanced instrumented indentation techniques helps to understand mechanical properties, phase distribution, and the effects of relative humidity on cement. By employing grid indentation, a deeper understanding of cement behavior at the micro- and nanoscale is achieved, revealing insights that traditional trial-and-error approaches cannot provide.

The grid indentation method allows for the characterization of mechanical properties across large areas, offering a detailed distribution of hardness and elastic modulus in multiphase cement samples (see Figure 12 and Figure 13). The study focused on two specific cement phases, requiring polished and smooth surfaces for accurate measurement. This technique also facilitated the determination of volume fractions of individual phases, a crucial factor in understanding material heterogeneity.

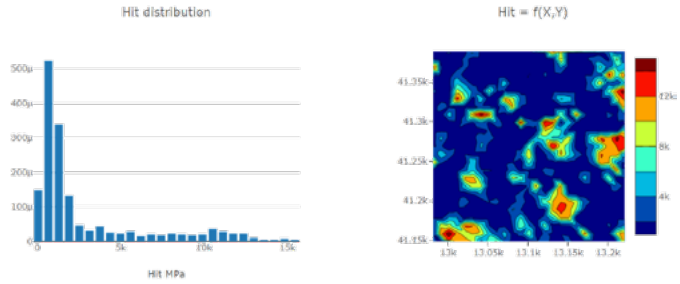

Figure 12: Distribution of hardness modulus.

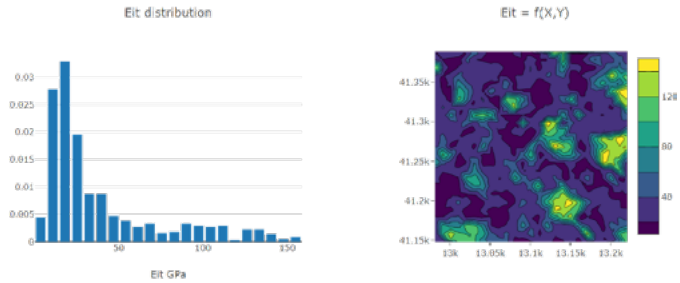

Figure 13: Distribution of elastic modulus.

	EIT [GPa]	HIT [GPa]	PHASE RATIO [%]
Phase 1	21.8	1.2	64.9
Phase 2	78.7	6.9	35.1

Table 8: Analyis of two phases.

Tests conducted in a controlled humidity chamber demonstrated that relative humidity significantly impacts cement properties. As humidity increased from 30 % to 90 %, both hardness and elastic modulus decreased, indicating that moisture weakens the mechanical properties of cement. These findings are critical for applications in environments with fluctuating humidity levels, where cement durability and performance are affected (see Figure 14).

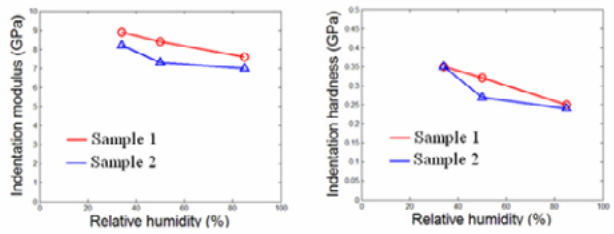

Figure 14: Hardness and elastic modulus measured in the range 30 % to 90 % relative humidity.

Cement hardening was evaluated using a specialized hardness tester. Measurements taken two hours after deposition showed progressive changes in hardness and elastic modulus, highlighting the dynamic nature of the hardening process even within the first few hours.

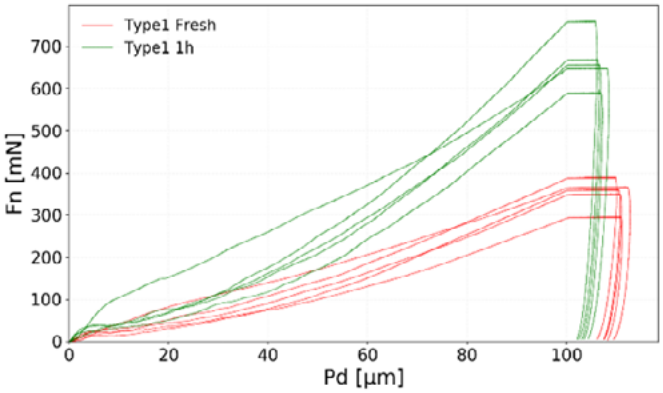

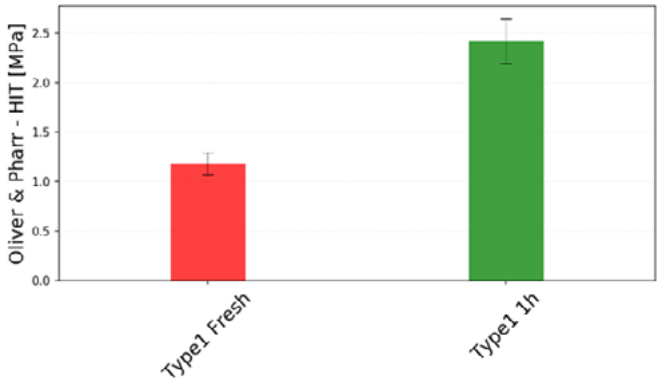

Figure 15: Cement hardening evaluation using hardness and elastic modulus.

These results underline the importance of micro- and nanoscale studies in cement research. The grid indentation method and controlled humidity testing provide a robust framework for assessing mechanical properties, understanding phase behavior, and exploring the effects of environmental conditions. This knowledge is essential for optimizing cement formulations and improving performance under various operating conditions.

INSTRUMENTS SUITABLE FOR THESE MEASUREMENTS

Step platform with MCT³ measuring head

1.9 MOISTURE ANALYSIS OF CEMENT

Moisture analysis using automated oven drying measures raw material moisture in a measuring range of >0.1 % and up to 99.9 % moisture content. The following table shows examples for test runs with various cement samples.

Residual moisture was monitored throughout the drying process, generating a drying curve that provides essential insights into the specific drying times of the cement. This critical parameter helps optimize processing and application. Additionally, moisture analysis ensures the quality of the cement by verifying the absence of residual moisture contamination, benefiting both producers and end-users.

INSTRUMENTS SUITABLE FOR THESE MEASUREMENTS
Brabender MT-CA

SAMPLE	INITIAL WEIGHT [g]	FINAL WEIGHT [g]	RESIDUAL MOISTURE	TEMPERATURE [°C]	DRYING TIME [min]
Cement 1	19.971	19.395	0.18 %	130	180
Cement 2	29.312	29.264	0.16 %	130	20
Cement 3	28.653	28.606	0.16 %	130	20
Cement 4	28.920	28.872	0.16 %	130	20
Cement 5	28.723	28.675	0.17 %	130	20

Table 9: Residual moisture values for different cement samples.

2 Characterization of Concrete

Concrete is a fundamental material in modern construction, providing the structural framework for everything from residential buildings to massive infrastructure projects. Its versatility and durability depend on understanding its physical and mechanical properties. Optimizing concrete production requires precise control over factors like phase composition, density, and microstructural characteristics, which determine its strength and durability.

This chapter highlights advanced methods like in-situ XRD for optimizing AAC production, skeletal density analysis for quality control, and nanoindentation for analyzing UHPC properties, showcasing techniques that enhance the performance of concrete in diverse construction applications.

2.1. QUALITY CONTROL AND MATERIAL OPTIMIZATION OF AAC WITH IN-SITU XRD

Analyzing quartz dissolution and tobermorite formation under hydrothermal conditions is crucial for optimizing the production and performance of autoclaved aerated concrete (AAC) and similar silicate-based materials. This process directly influences the material's strength, durability, and thermal properties by controlling the formation of tobermorite, a key phase responsible for these attributes. Understanding these reactions helps refine manufacturing conditions.

To monitor quartz dissolution and tobermorite formation under hydrothermal conditions, XRD with a reflection setup in an autoclave chamber can be used. This technique allows the gaining of information for time-resolved phase quantification as well as additional spatial information on the nature of the hydrothermal reactions at interfaces – thus optimizing the final material properties.

The test sample was prepared analogously to industrial autoclave aerated concrete (AAC) production with a water-to-solid ratio of 0.73 and 48.3 % quartz (99.1 % SiO_2; D50 23 µm), 38.1 % ordinary Portland cement, 8.7 % lime (93 % CaO), 5.0 % calcium fluorite (>99 %; sintered at 973 K for 3 h) and 0.1 % aluminum powder. Calcium fluorite is only added as an internal standard and is usually not found in AAC.

The autoclave chamber was preheated (<363 K) using the circulation thermostat after placing the sample in the chamber. After flushing the chamber with saturated water vapor, the vent was sealed (0 min) to allow pressure to build up. By steadily increasing the boiler and thermostat temperature, hydrothermal conditions at 466 K and 1.35 MPa were obtained (230 min). After a reaction period of 5.7 h, the steam supply boiler was switched off (570 min) and the system cooled down slowly.

The comparison of the measured diffractograms (Figure 16) shows a decrease of the quartz 101 reflection intensity and an increase of the tobermorite 110 reflection intensity, while the fluorite 111 reflection serves as an internal standard.

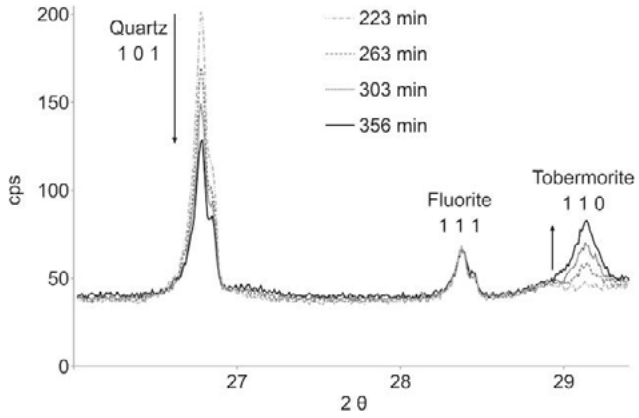

Figure 16: Diffractograms taken between 26° and 29.3° 2θ, close to and after reaching constant hydrothermal conditions at 466 K and 1.35 MPa (>230 min).

Below 443 K, the normalized intensities (Figure 17) show a proportional decrease of quartz and fluorite with increasing time and thus temperature. The steam density inside the autoclave chamber changes from 0.59 kg m^{-3} at 373 K to 6.86 kg m^{-3} at 466 K and leads to an increase in X-ray absorption[4]. Above 443 K, the quartz peak decreases much faster than the fluorite peak; this marks the beginning of hydrothermal dissolution. The tobermorite peak starts to increase >443 K. Both the decrease of the quartz peak and the increase of the tobermorite peak can be approximated with first-order reaction behavior (solid lines in Figure 17) after applying temperature corrections. As evidenced by

earlier studies, tobermorite formation occurs via poorly crystalline calcium silicate hydrates and is initially limited by the dissolution of quartz[5].

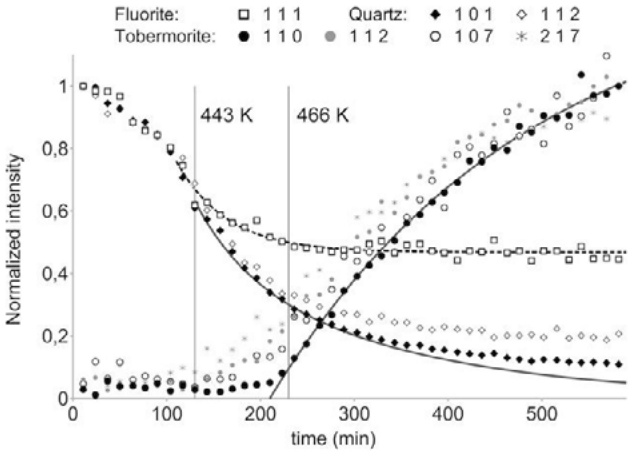

Figure 17: Normalized reflection intensities from 373 K to constant conditions at 466 K at 1.35 MPa. The approximation (solid line) is a combination of temperature correction (dashed line) and first-order behavior.

The reflection setup of the autoclave chamber used here is suitable for monitoring hydrothermal reactions in-situ. It can provide routine information for time-resolved phase quantification as well as additional spatial information on the nature of the hydrothermal reactions at interfaces due to the surface sensitivity of the reflection geometry.

INSTRUMENTS SUITABLE FOR THESE MEASUREMENTS

XRDynamic 500

2.2 SKELETAL DENSITY DETERMINATION OF CONCRETE

A critical property of concrete is its skeletal density, which helps monitor material quality from raw powders to the final product and facilitates volume-to-mass conversions for sales. In this study, the skeletal density of a commercially available concrete patcher was analyzed using a gas pycnometer.

A 157.31 g sample of concrete patcher was placed in a large sample cell and prepared with a one-minute helium flow purge before measurement. The analysis was conducted using helium gas, with detailed parameters shown in Table 10.

PARAMETER	SETTING	PARAMETER	SETTING
Sample cell	Large	Target pressure	10 psig
Analysis gas	Helium	Flow mode	Fine powder
Temperature	25 °C	Number of runs	15
Preparation	Flow, 1 min	Runs to average	5
Flow direction mode	Reference first	End mode criteria	Better than 0.0025 %
Equilibration mode	Temperature and pressure		

Table 10: Concrete measurement parameters.

The measured skeletal density of the concrete patcher was 2.7477 g/cm³ (2747.7 kg/m³), as depicted in Figure 18. The sample volume was calculated from pycnometry experiments using Boyle's Law. These results confirmed the instrument's precision in determining skeletal density, a key parameter for quality control and material evaluation.

Results

True Density

2.7477 g/cm³

Average Volume

57.251 cm³

Percent Variance

0.0020 %

Run Data

Run	Volume	Density	Temperature
1	57.400 cm³	2.7406 g/cm³	25.008 °C
2	57.271 cm³	2.7468 g/cm³	24.996 °C
3	57.262 cm³	2.7472 g/cm³	24.995 °C
4	57.255 cm³	2.7475 g/cm³	24.997 °C
5	57.250 cm³	2.7478 g/cm³	25.000 °C
6	57.252 cm³	2.7477 g/cm³	25.000 °C
7	57.241 cm³	2.7482 g/cm³	24.999 °C
8	57.243 cm³	2.7481 g/cm³	24.998 °C
9	57.250 cm³	2.7478 g/cm³	25.000 °C
10	57.250 cm³	2.7478 g/cm³	25.000 °C
11	57.252 cm³	2.7477 g/cm³	24.998 °C

Figure 18: Helium gas pycnometry on concrete mix.

INSTRUMENTS SUITABLE FOR THESE MEASUREMENTS

Ultrapyc Series

3 Analysis of Metals

The exceptional mechanical properties of metals, such as strength, ductility, and conductivity make them indispensable for creating durable and efficient structures and components. However, ensuring the long-term performance of metals often requires a deep understanding of their behavior under various environmental and operational conditions.

Key aspects of metal performance, such as corrosion resistance, hardness, and mechanical stability, are influenced by factors including composition, surface treatments, and environmental exposure. Advanced analytical techniques allow for precise characterization of these properties, enabling manufacturers to optimize metal formulations, improve surface treatments, and develop protective coatings for enhanced durability.

In this chapter, we explore the analytical tools and methods used to assess and enhance the performance of metals. Topics include corrosion inhibition, mechanical property analysis, and the role of protective coatings in extending the lifespan of metal components. By understanding these properties at a microscopic level, manufacturers can ensure metal components meet rigorous standards for reliability and sustainability in even the most demanding applications.

3.1 CORROSION INHIBITION OF STAINLESS STEEL BY PROTECTIVE COATING

To enhance its longevity in corrosive conditions like seawater exposure, protective coatings are applied. The zeta potential is a critical surface parameter for assessing the effectiveness and quality of these coatings. It provides insights into surface chemistry and conductivity, essential for understanding corrosion phenomena.

Streaming current measurements accurately determine the zeta potential of stainless steel, unaffected by its intrinsic metal conductivity. In contrast, streaming potential measurements yield lower apparent zeta potentials as they overlook surface conductivity. Experiments with stainless steel plates coated with various materials revealed a decrease in surface conductance in the order: uncoated > DLC (diamond-like carbon) ~ SICAN (silicon-doped DLC) > SICON (silicon oxide-doped DLC). The SICON coating, with identical correct and apparent zeta potential values, demonstrated an insulating surface, effectively inhibiting corrosion.

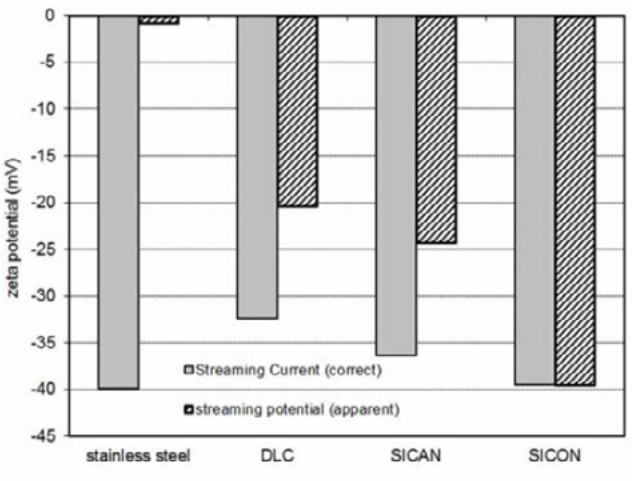

Figure 19: Zeta potential obtained by streaming current and streaming.

These measurements, conducted in 10^{-3} M KCl at pH 5.5, validate the ability of streaming current and potential techniques to characterize and compare coatings, ensuring optimal corrosion resistance in demanding environments.

INSTRUMENTS SUITABLE FOR THESE MEASUREMENTS
SurPASS 3

3.2 HARDNESS EVOLUTION IN STEEL WIRES FOR BRIDGE ANCHORS

This chapter investigates the mechanical properties of steel wire strands used in bridge anchors by performing nanoindentation measurements in a radial matrix. The samples, embedded in resin and polished, were tested at specific radial distances from the center of the strands. Each point in the matrix represents an indentation measurement, with five measurements taken at the center for accuracy.

The results (see Table 11, Table 12 & Figure 20) showed that both hardness and elastic modulus were lower near the center of the strands and increased toward the edges. This gradient suggests that the material is slightly harder and stiffer closer to the surface, a trend more pronounced for the elastic modulus. The relative increase in modulus between the center and the edge was 18 % for Sample A, 27 % for Sample C, and 12 % for Sample B. For hardness, the increase was less significant, with Sample A showing a 9 % increase compared to 5.7 % for Sample B and 4.9 % for Sample C.

SAMPLE		CENTER	R 0.5	R 1.0	R 1.5	R 1.85	R 2.02	R 2.19	R 2.34	R 2.48
A	Mean	6.10	6.22	6.36	6.46	6.64	6.51	6.43	6.65	6.69
	Standard deviation	0.20	0.21	0.14	0.21	0.22	0.24	0.30	0.19	0.30
B	Mean	6.13	6.12	6.30	6.46	6.45	6.41	6.36	6.60	6.48
	Standard deviation	0.27	0.14	0.25	0.20	0.18	0.21	0.26	0.18	0.14
C	Mean	6.39	6.36	6.26	6.44	6.46	6.49	6.45	6.34	6.71
	Standard deviation	0.38	0.21	0.30	0.27	0.20	0.16	0.18	0.30	0.22

Table 11: Results - Hardness [GpPa].

SAMPLE		CENTER	R 0.5	R 1.0	R 1.5	R 1.85	R 2.02	R 2.19	R 2.34	R 2.48
A	Mean	194.75	200.96	220.87	226.33	229.58	224.54	228.58	227.69	230.19
	Standard deviation	3.09	14.02	6.97	5.73	6.80	6.05	7.06	4.72	10.64
B	Mean	175.16	198.63	213.69	222.46	221.44	225.51	222.97	229.60	222.95
	Standard deviation	3.64	21.74	17.05	16.74	17.37	16.97	15.44	18.06	21.13
C	Mean	189.87	188.18	202.57	208.73	207.57	211.93	208.52	208.82	213.71
	Standard deviation	5.12	16.01	23.25	20.74	24.03	22.84	24.90	23.39	22.33

Table 12: Results - Elastic modulus [GPa].

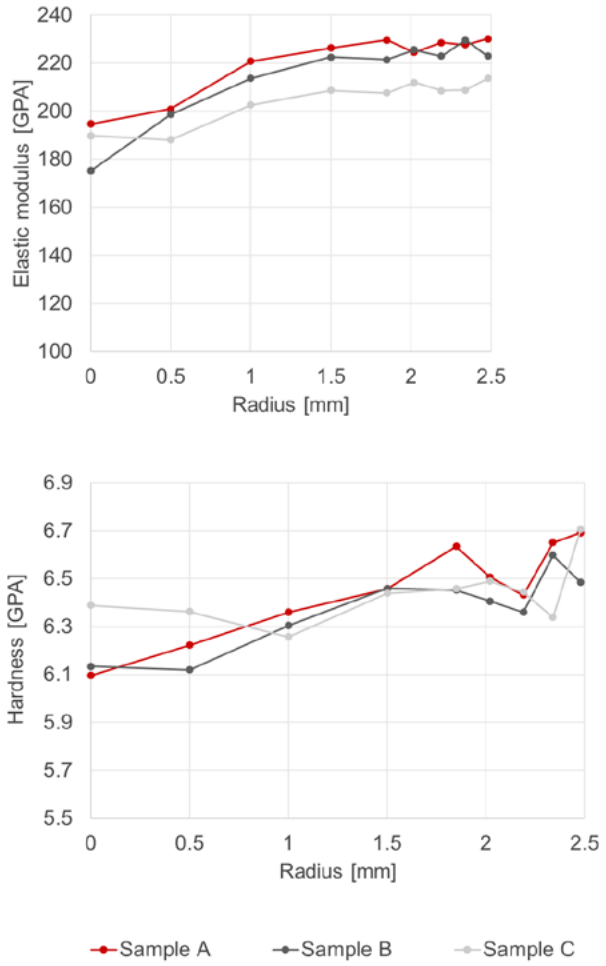

Figure 20: Data curves of hardness and elastic modulus.

The data demonstrated good repeatability, with a standard deviation of 5 % to 10 %, though higher variability was observed for Sample C and elastic modulus measurements. The gradient in mechanical properties may result from stress fields caused by wear during use or environmental interactions affecting the surface over time. This insight is crucial for understanding the durability and performance of anchor cables under operational conditions.

INSTRUMENTS SUITABLE FOR THESE MEASUREMENTS

Step platform with NHT³ measuring head

3.3 MICROWAVE DIGESTION OF STEEL AND ALLOYS FOR ICP ANALYSIS

The precise and accurate determination of alloying constituents in steels and nickel-based alloys is analytically demanding, but of great technical and commercial significance for steel and high-performance metal industries.

Closed-vessel microwave digestion using Multiwave 5001 followed by ICP-OES analysis provides an accurate and reliable solution. This wet-chemical method of analysis is used as an arbitration procedure as well as an important calibration method for X-ray spectrometers to ensure high accuracy.

In order to demonstrate the excellent suitability of Multiwave 5001 for sample preparation of metal samples prior to element analysis, the recovery rates of certified reference materials were determined.

Four standard reference materials were chosen for examination based on their properties and relevancy in the steel and metal industry (Table 13).

SAMPLE NAME	DESCRIPTION
BCS090-1	1 % Carbon steel (not alloyed)
BCS179-2	Alloyed steel 1.2550
BCS295-1	High alloyed steel
BCS-CRM346	Nickel-based alloy

Table 13: Samples digested and analyzed in this study.

Multiwave 5001 offers the well-established SmartVent technology at an advanced temperature level of up to 250 °C, thus providing excellent digestion quality for hard-to-digest metals requiring higher temperatures.

The weighed amount of 200 mg was digested successfully with aqua regia and a small amount of hydrofluoric acid. The recorded data of the digestion run is displayed in Figure 21.

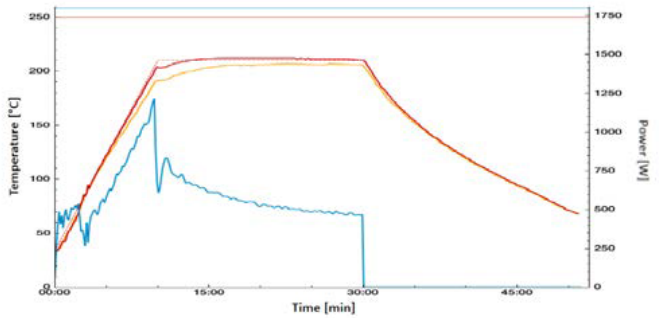

Figure 21: Run data.

The quantitative analysis was performed on an ICP-OES – results for one sample (high alloyed steel) are displayed in Table 14.

ELEMENT	CERTIFIED VALUE	FOUND VALUE	RECOVERY
	%	%	%
Cr	19.51 ± 0.06	18.79 ± 0.98	96
Mo	3.996 ± 0.024	3.637 ± 0.116	91
Ni	24.40 ± 0.04	23.99 ± 0.92	98
V	0.0456 ± 0.0015	0.0442 ± 0.0008	97
Mn	1.758 ± 0.009	1.737 ± 0.066	99
Cu	1.461 ± 0.012	1.352 ± 0.058	93
Co	0.045 ± 0.001	0.046 ± 0.006	103

Table 14: BCS295-1, high alloyed steel, results with standard uncertainties (n=5).

Multiwave 5001 equipped with Rotor 20SVT50 is a powerful configuration for the fast and reliable digestion of steel and high-performance nickel alloy samples. The applied method is not only suitable for the digestion of the mentioned reference materials but also serves as a representative starting point for any kind of steel or high-performance alloy sample.

SUITABLE INSTRUMENTS

Multiwave 5001

Multiwave 7501

3.4 CAUSTIC LEACHING OF BAUXITE FOR PROCESS SIMULATION OF THE BAYER PROCESS

Small-scale bauxite leaching is performed in the refinery laboratory to simulate the caustic leaching of the Bayer process, which is used globally for separation of pure alumina (Al_2O_3). The goal of this leaching is to determine the amount of "available alumina" in the bauxite ore. The amount of "reactive silica" is normally assessed too for cost reasons, as it consumes a considerable amount of NaOH.

The contents of alumina and silica are traditionally determined in small-scale high-pressure steel bombs, in which it is difficult to control the heating to target temperature and to maintain it. Thus, microwave heating offers an attractive way to efficiently control the process.

This study shows the reproducibility of the simulated extraction in Multiwave 7301 in 30 mL PTFE vials, using NIST SRM 600. NIST SRM 600 is the only commercially available bauxite reference material and comes from the Western Australian Darling Range. It is certified for XRF total contents of Al (40.0 %) and Si (20.3 %), while the extraction efficiencies of Al_2O_3 are about 80 % and for SiO_2 as low as 8 % to 10 %.

To ensure homogenous temperature distribution, effective stirring by the built-in magnetic stirring device is required.

The following steps need to be conducted for the process simulation:

1. 1 g Bauxite sample – add 10 mL 8 % NaOH and stir bar.
2. Microwave heating in 30 min to 230 °C, hold for 30 min.
3. Transfer into 50 mL centrifuge vials with standing rim, transfer stir bar as well.
4. Dilute to ~ 20 mL with H_2O (DI) while stirring.
5. Leave some rinse solution in the digestion vial and acidify with 1.3 mL H_2SO_4 conc., transfer into the stirred 50 mL vial and make sure that the sediment is thoroughly mixed.
6. Fill to 50 mL and continue stirring for about 10 min.
7. Transfer 1 mL of the solution into 15 mL centrifuge vial, remove stir bar.
8. Add ~ 3 mL H_2O (DI), centrifuge (3,000 m^{-1} for 15 min), decant and collect centrifugate.
9. Repeat with fresh 3 mL H_2O (DI), and combine both centrifugates.
10. Fill up to 10 mL with H_2O (DI) for measurement.

Calibration solutions were also prepared in the matrix matched rinse solution. Al was monitored at 308.215 nm and 309.271 nm. The latter line was used for quantification. For Si the more sensitive line at 251.612 nm was used below 50 ppm only. For higher concentrations the less sensitive line at 152.672 nm was used.

At 230 °C the concentration of Al_2O_3 was measured as 35.03 % and 11.53 % for SiO_2 (Figure 22). Further, the important standard deviation of nine replicate digestions was as low as 0.58 % for Al_2O_3 and 0.60 % for SiO_2. Multiwave 7301 is a valuable method to leach alumina and silicate from bauxite in order to simulate the Bayer process.

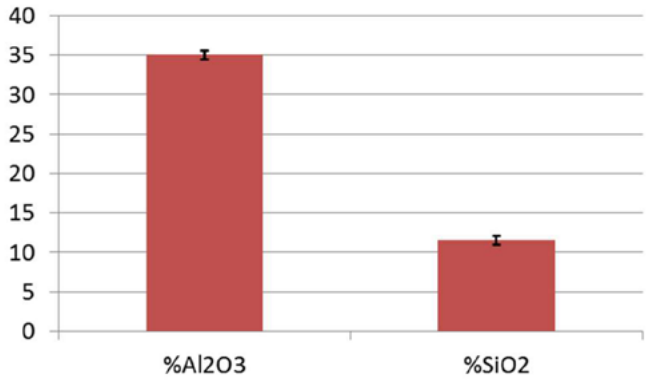

Figure 22: Concentration of Al_2O_3 and SiO_2 and precision indicators for nine replicated extractions of NIST SRM 600 bauxite.

SUITABLE INSTRUMENTS
Multiwave 5001
Multiwave 7101/7301/7501

4 Analysis Methods for Other Common Building Materials

Beyond cement and metals, materials such as glass, wood, and architectural finishes like plasters, coatings, and ceramic tiles play vital roles in modern construction. These materials not only enhance the functionality and aesthetics of structures but also contribute to durability, energy efficiency, and environmental sustainability. Each of these materials presents unique challenges in production and application, requiring precise analytical methods to optimize their performance.

This chapter explores advanced analytical techniques for evaluating these diverse materials. From dynamic mechanical analysis and rheological testing to surface characterization and wear resistance studies, these methods provide manufacturers with the tools to develop high-performance building materials, ensuring quality, efficiency, and aesthetic appeal in modern construction projects.

4.1 GLASS

4.1.1 Rheological investigation of glass

In the glass industry, understanding viscosity as a function of temperature is essential for optimizing production processes, ensuring product quality, and developing innovative materials. Viscosity governs critical stages such as forming, shaping, and refining. It also helps identify key thresholds like crystallization and devitrification points, allowing manufacturers to adjust cooling rates and improve efficiency and yield.

Viscosity measurements were conducted on optical glass and high-melting lithium aluminum silicate glass. The viscosity curve for optical glass (Figure 23) was obtained at cooling rates of 5 °C/min, 2.5 °C/min, and 1 °C/min. The 5 °C/min curve followed a typical VFT (Vogel-Fulcher-Tammann) behavior, characteristic of non-crystallizing glass melts. Slower cooling rates revealed significant deviations at lower temperatures, with crystallization thresholds below 1,100 °C for 1 °C/min and 1,050 °C for 2.5 °C/min. These findings demonstrate how cooling rates influence viscosity and material properties, impacting product quality.

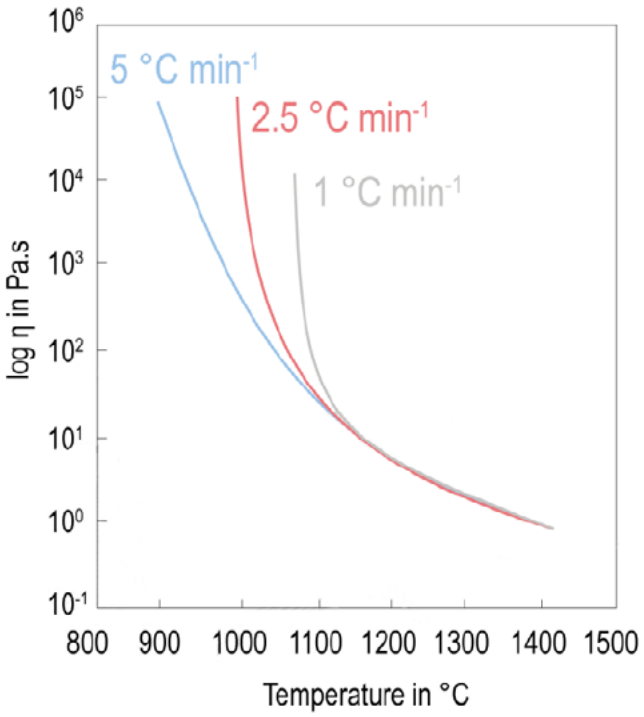

Figure 23: Viscosity plot for optical glass for three different cooling rates.

For high-melting glass, viscosity was measured up to 1,750 °C (Figure 24). The curve was smooth and reproducible, showcasing the potential to establish a glass reference material. Such a reference requires homogeneity in the utilized batch, ideally sourced from large-scale production.

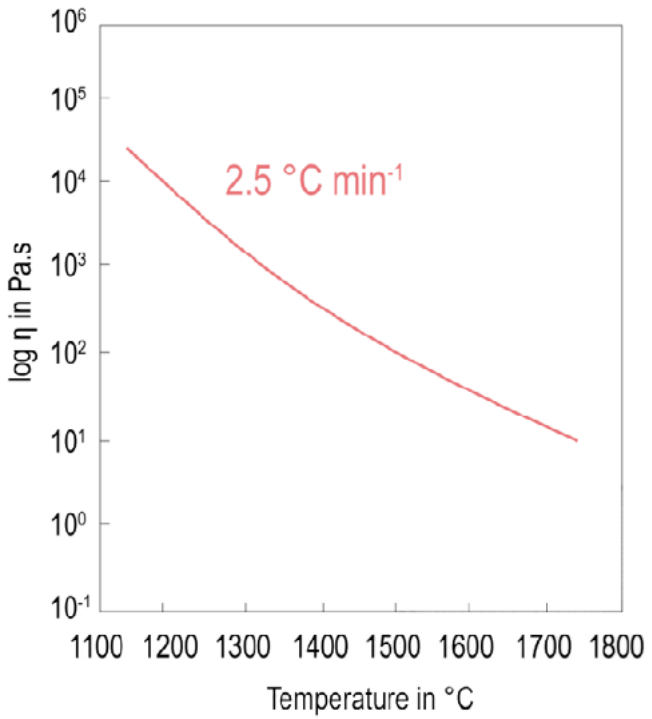

Figure 24: Viscosity curve of high-melting glass up to 1,750 °C.

These results highlight the necessity of precise viscosity measurements to control manufacturing processes and prevent defects such as crystallization. The ability to adjust cooling rates based on viscosity data improves product yield and operational efficiency. The study also emphasizes the importance of high-sensitivity equipment to achieve reliable and reproducible measurements across wide temperature ranges. This data is crucial for material modeling and simulations, enabling manufacturers to optimize both quality and productivity. The integration of viscosity data into production workflows ensures that glass meets the demanding standards of modern applications.

INSTRUMENTS SUITABLE FOR THESE MEASUREMENTS
FRS Series

4.1.2 Rheological investigations of glass for glass wool production

Glass wool production is a highly energy-intensive process where understanding the viscosity of molten glass is critical for optimizing manufacturing, enhancing product quality, and reducing costs. Viscosity affects process stability, material flow behavior, and fiberization during production, directly impacting the insulation value of the final product. Insights into temperature- and shear-rate-dependent viscosity allow manufacturers to adjust process parameters, lower energy consumption, and improve the precision of equipment design.

Viscosity measurements were performed on borosilicate glass, the base material for glass wool, at temperatures of 1,000 °C, 1,100 °C, and 1,200 °C, and shear rates ranging from 1 s^{-1} to 20 s^{-1}. The results, depicted in Figure 25, showed clear Newtonian behavior, with viscosity remaining constant across the tested shear rates at a given temperature. The viscosity decreased significantly with increasing temperature, from 161 Pa·s at 1,000 °C to 18 Pa·s at 1,200 °C, demonstrating strong temperature dependence.

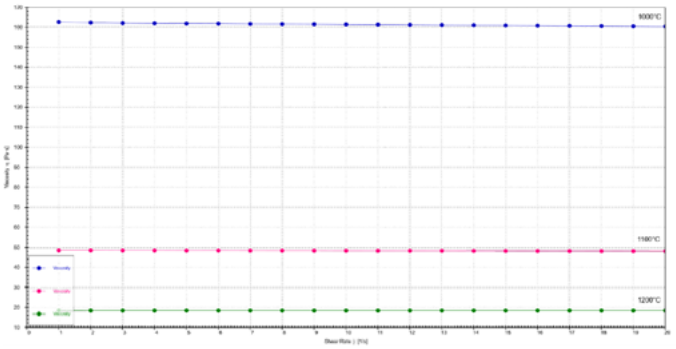

Figure 25: Viscosity of molten borosilicate glass at 1,000 °C, 1,100 °C and 1,200 °C and at different shear rates showing Newtonian behavior.

During the cooling phase (Figure 26), viscosity was monitored at a constant shear rate of 7 s^{-1}. The data revealed precise changes in viscosity within the 1,200 °C to 1,000 °C range, critical for the fiberization stage. Finer fibers, which improve insulation by trapping more air, are directly linked to controlled viscosity during this phase.

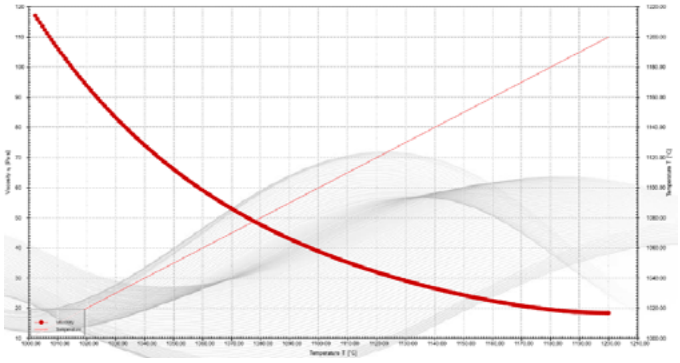

Figure 26: Viscosity of molten borosilicate glass at a constant shear rate of 7 s^{-1} during the cooling process from 1,200 °C down to 1,000 °C.

The findings highlight the importance of viscosity in optimizing glass wool production. Accurate viscosity data enable manufacturers to lower process temperatures, saving energy and reducing costs. Adjusting the viscosity also minimizes maintenance requirements by improving material flow through nozzles and fiberizing disks. Furthermore, precise control over viscosity enhances the insulation value of glass wool by ensuring optimal fiber formation. This understanding supports not only operational efficiency but also the development of new, high-performance glass wool materials. The ability to adapt to variations in raw material composition, particularly recycled glass, ensures consistent product quality in a competitive industry.

INSTRUMENTS SUITABLE FOR THESE MEASUREMENTS

FRS Series

4.1.3 Dynamic mechanical analysis of glass

Dynamic mechanical analysis (DMA) is essential for characterizing the viscoelastic properties and phase transitions of glass at high temperatures. Understanding properties such as storage modulus, loss modulus, and extensional viscosity aids in optimizing manufacturing processes, selecting materials for specific applications, and predicting performance under thermal stress. These measurements are crucial for ensuring product quality, durability, and suitability for intended applications.

The study analyzed three types of industrial glasses: optical glass, alumosilicate glass (technical glass 1), and alkaline earth alumosilicate glass (technical glass 2). Temperature ramps (Figure 27) revealed distinct differences in viscoelastic behavior and softening points. Optical glass exhibited the lowest storage modulus (~53.5 GPa) and softened at ~400 °C. Technical glass 1 softened around 500 °C with a storage modulus of ~65.2 GPa, while technical glass 2 had the highest storage modulus (~91.8 GPa) and softened above 770 °C.

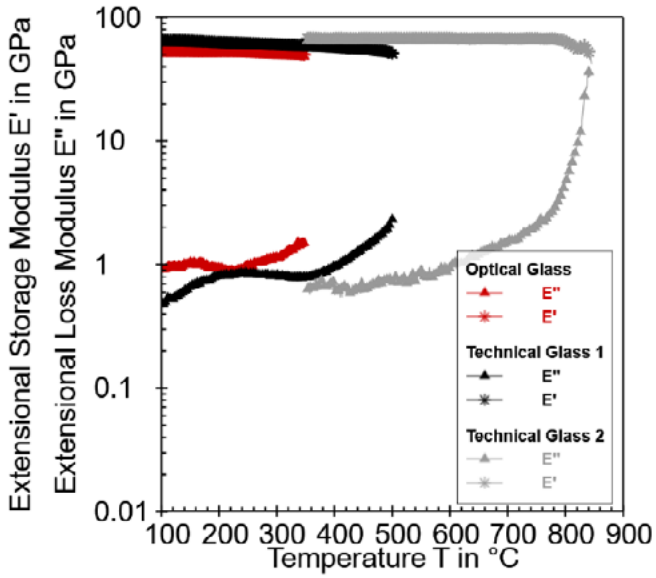

Figure 27: Comparison of the storage and loss moduli of the three glasses.

Extensional viscosity, measured through beam bending tests according to ISO 7884-4, confirmed these trends. As shown in Figure 28, optical glass reached softening at the lowest temperature (~400 °C), followed by technical glass 1 (~500 °C) and technical glass 2 (~800 °C). Viscosity values aligned with dynamic measurements, highlighting the temperature dependence of flow behavior.

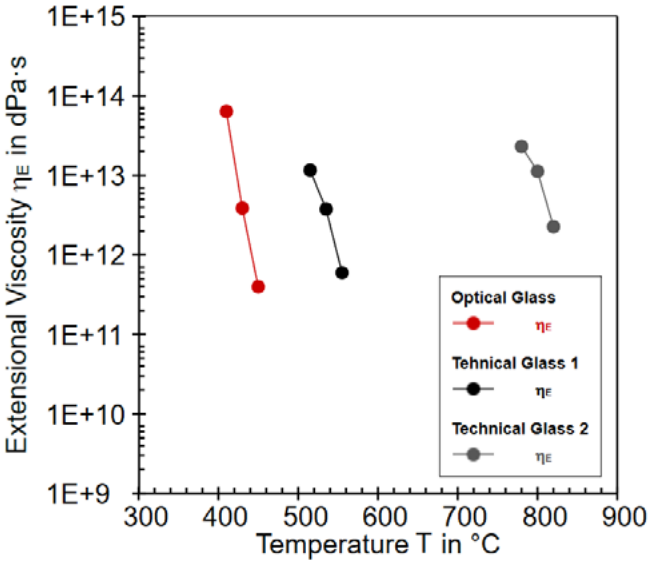

Figure 28: Comparison of the viscosity of the three glasses according to ISO 7884-4.

The results provide critical insights into the thermal and mechanical behavior of different glass compositions. Storage modulus (E') values and viscosity data guide material selection for applications requiring specific operating temperature ranges. The glass transition temperature (Tg) informs annealing conditions, thermal stability, and susceptibility to changes like crystallization. Reproducibility tests (Figure 28) demonstrated reliable measurement consistency, validating the methodology.

INSTRUMENTS SUITABLE FOR THESE MEASUREMENTS
MCR 702e MultiDrive

4.2 WOOD

4.2.1 Humidity-dependent properties of adhesives used in wood construction

Understanding the effect of humidity on the elastic modulus of adhesives is critical for wood construction, where bonded components are exposed to varying climatic conditions. Moisture absorption can alter adhesive properties, leading to relaxation effects, changes in viscoelastic behavior, and potential mismatches between the elastic moduli of wood and adhesives. This can compromise fracture toughness and joint integrity. Accurate and efficient measurement methods are essential for characterizing adhesives, ensuring durability, and optimizing formulations for specific applications.

The tensile elastic modulus of three adhesives – 1K-PUR, MUF, and PRF – was tested under varying humidity levels (30 %, 50 %, 65 %, and 80 %) at 20 °C. Results in Figure 29 showed a general trend where increased humidity led to a reduction in the elastic modulus for 1K-PUR and PRF, aligning with literature values. MUF, however, exhibited no significant change, which could be attributed to variations in melamine content that enhance hydrolysis resistance. The measured values closely matched existing reference data, confirming the method's accuracy despite thinner sample films and faster conditioning times.

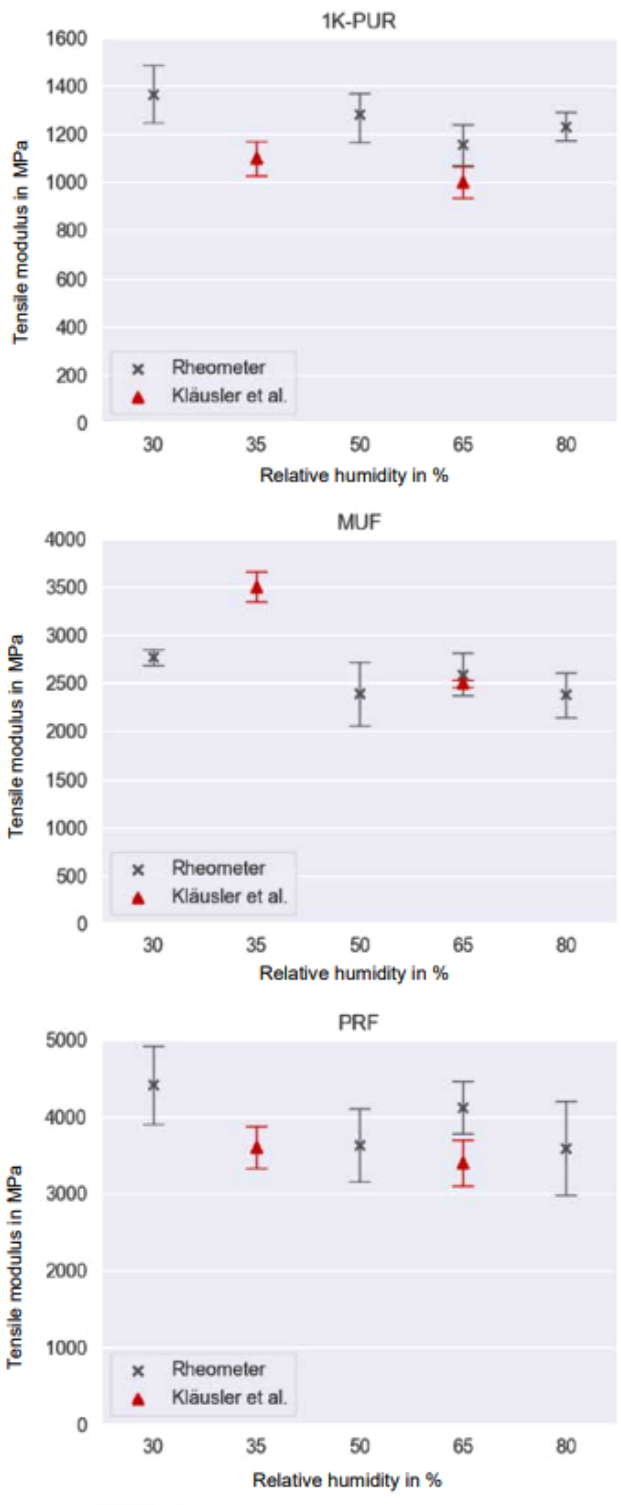

Figure 29: Mean values and standard deviations of the tensile tests at 20 °C. Additionally, results reported by Kläusler et al[5] are shown for measurements at 23 °C.

Table 15 highlights the coefficient of variation (CV) for the measurements. For 1K-PUR and PRF, the CVs were within expected ranges, indicating reliable data. For MUF, the higher CV was linked to brittleness and potential micro-cracks in the samples, detectable only under microscopic inspection.

INSTRUMENTS SUITABLE FOR THESE MEASUREMENTS
MCR 702e MultiDrive

ADHESIVE DATA / GLUE	1K-PUR	MUF	PRF
Rheometer	7.4	8.7	8.2
Kläusler et al.	6.6	1.6	8.9

Table 15: Coefficient of variation of the measured elastic moduli in % in a climate of 20 °C with 65 % relative humidity.

These findings demonstrate the effectiveness of a rapid, climate-controlled tensile testing method for assessing adhesive properties. The observed reduction in elastic modulus at higher humidity levels suggests the need for formulations that can maintain structural performance under moist conditions. Variations between adhesive types underscore the importance of tailoring compositions, such as melamine content, to specific environmental demands.

This accelerated method provides reliable data while significantly reducing test times compared to traditional approaches. It is particularly beneficial for quality control, enabling manufacturers to adapt adhesives to dynamic environmental conditions and ensure consistent product performance.

4.2.2 Scratch resistance of self-healing paints on wood

Paints and varnishes play a dual role in protecting and enhancing the appearance of wood and other materials. However, mechanical damage, such as scratches, can compromise their protective function, leading to material exposure and accelerated wear. Self-healing paints offer a promising solution by repairing scratches autonomously or with external stimuli like heat or light. Measuring scratch resistance and elastic recovery is critical to evaluate the performance of self-healing paints compared to conventional coatings and to quantify their ability to maintain aesthetics and durability under mechanical stress.

Scratch tests were performed on one self-healing and two conventional paints (on walnut and parquet) using a progressive load from 0.05 N to 30 N. Panorama images of scratches (Figure 30) showed no visible cracks, indicating that none of the coatings experienced critical failure under the test conditions.

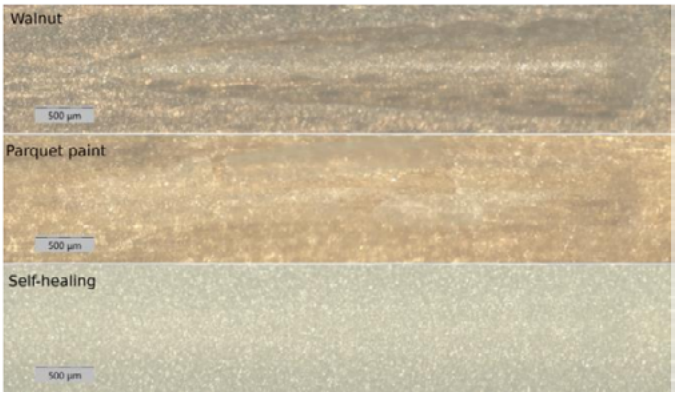

Figure 30: Panorama images of progressive load scratch on walnut, parquet, and self-healing paints. Thanks to excellent recovery the scratch is almost invisible on the self-healing paint.

However, significant differences were observed in elastic recovery. Self-healing paint exhibited an elastic recovery (ER) of ~80 %, substantially higher than walnut and parquet paints, which ranged between 40 % and 60 % (Figure 31).

Figure 31: Elastic recovery (ER) of the parquet, walnut and self-healing paint.

The superior recovery of self-healing paint was attributed to its ability to reduce residual depth post-scratch (Figure 32).

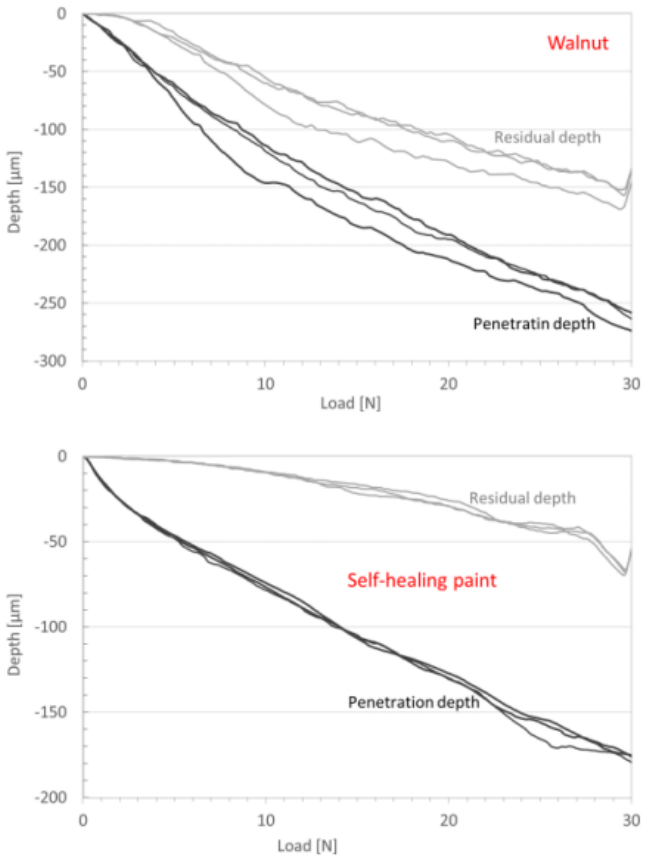

Figure 32: Comparison of penetration and residual depth on the walnut paint (top) and self-healing paint (bottom).

Instrumented indentation provided further insights into mechanical properties. Depth profiles of elastic modulus (Figure 33) revealed that self-healing paint showed an initial increase in modulus before reaching a plateau (~2.8 GPa), while conventional paints exhibited a steady decrease to ~2 GPa. Single-load indentation demonstrated consistent elastic recovery in self-healing paint (~34 %) regardless of applied load, contrasting with reduced recovery in walnut and parquet paints at higher loads (~20 %).

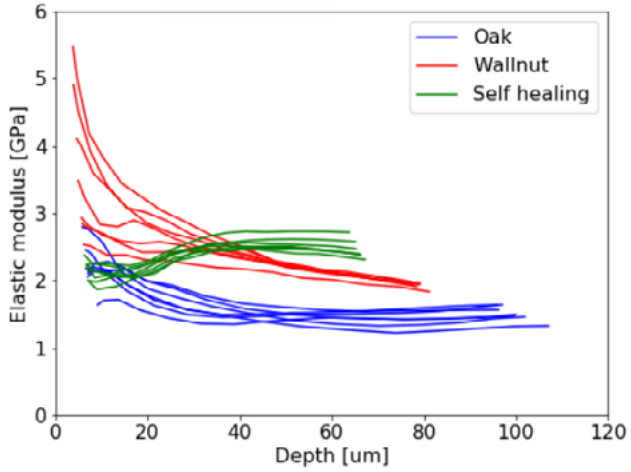

Figure 33: Depth profile of elastic modulus: note significantly different depth profile for the self-healing paint (green line).

The findings highlight the enhanced scratch resistance and elastic recovery of self-healing paints compared to conventional coatings. The high elastic recovery of self-healing paints indicates their ability to maintain surface integrity and appearance even under mechanical stress, reducing the need for frequent repainting. Instrumented indentation confirmed their superior mechanical properties, including consistent recovery across varying deformation levels. These measurements validate the effectiveness of self-healing paints in extending the lifespan and functionality of coated wood surfaces, making them a viable choice for high-demand applications.

INSTRUMENTS SUITABLE FOR THESE MEASUREMENTS
Step platform with MCT³ | NST³ measuring heads

4.2.3 Surface charge determination of wood

The surface charge of lignocellulosic materials, indicated by the zeta potential, is critical for understanding properties like hydrophilicity, swelling, and surface functionalization. These characteristics influence material performance in applications such as lightweight composites, textiles, and reinforced fibers. For wood, surface charge measurements help assess compatibility with adhesives, coatings, and polymer matrices, enabling optimization for mechanical strength and durability. The zeta potential also reveals interfacial changes caused by chemical or physical modifications, providing a tool to enhance wood's performance and longevity.

The study investigated the zeta potential of hardwood (beech) and softwood (spruce) in various forms – wood, pulp, and regenerated cellulose fibers.

Zeta potential and swelling: Figure 34 illustrates that wood, pulp, and cellulose fibers exhibited negative surface charges across a wide pH range. Beech wood showed an isoelectric point (IEP) at pH 2.6, indicating carboxylic acid groups on the surface. Pulp displayed increased swelling at alkaline pH, evidenced by a maximum negative zeta potential. Regenerated cellulose fibers exhibited higher negative charge density, reflecting surface oxidation and impurity removal.

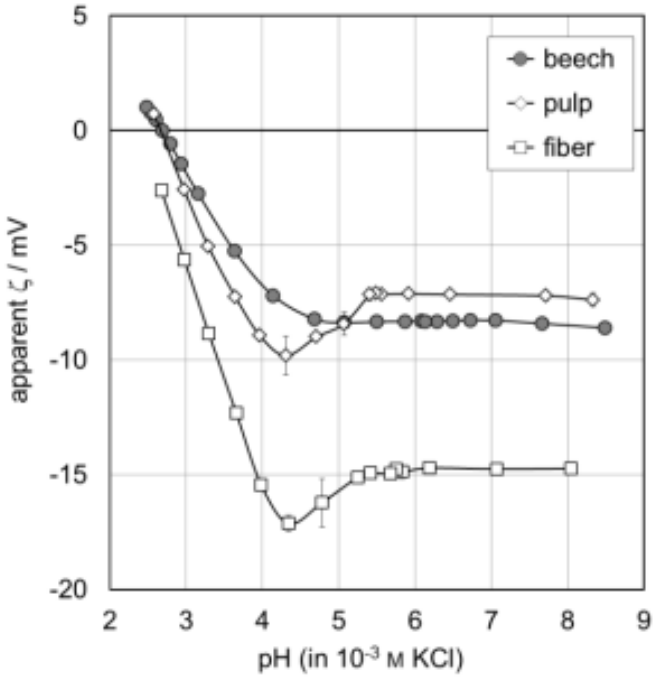

Figure 34: pH dependence of the apparent zeta potential for wood (beech), pulp, and regenerated cellulose fiber.

Hardwood vs. softwood: Beech (hardwood) had a more negative zeta potential compared to spruce (softwood), suggesting greater hydrophilicity due to denser functional groups:

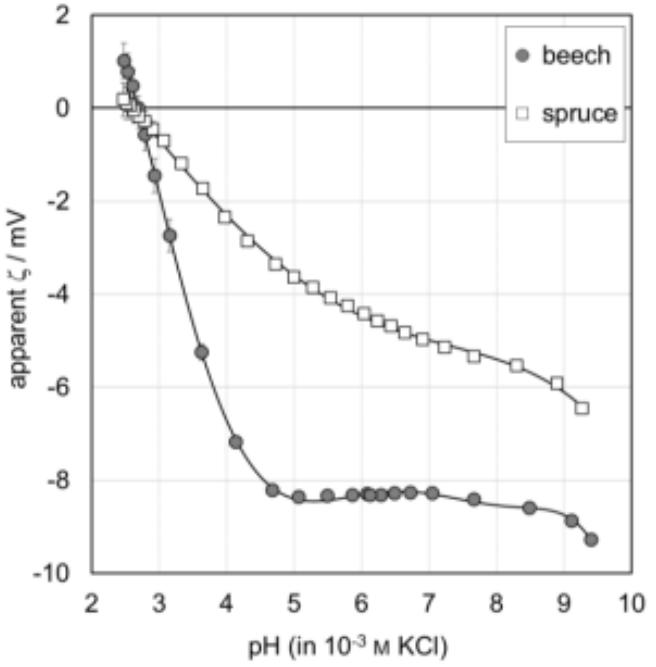

Figure 35: Comparison of zeta potential for hardwood (beech) and softwood (spruce) samples.

This difference became more pronounced above pH 4, where spruce showed slower swelling rates (Figure 36).

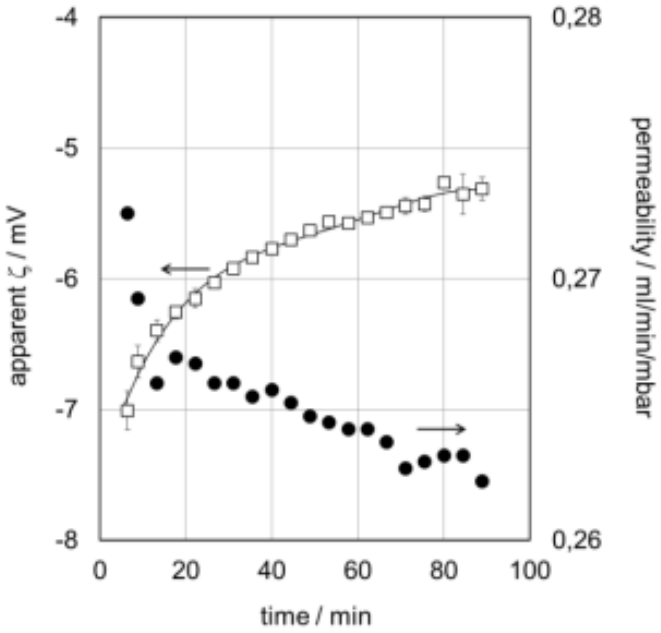

Figure 36: Swelling of spruce indicated by the change of zeta potential with time of exposure to an aqueous solution of 0.001 mol/l KCl at pH 6.2.

Functional group density: A titration method using cationic polyelectrolytes revealed higher surface functional group density in hardwood pulp compared to softwood, correlating with higher hydrophilicity (see Figure 37).

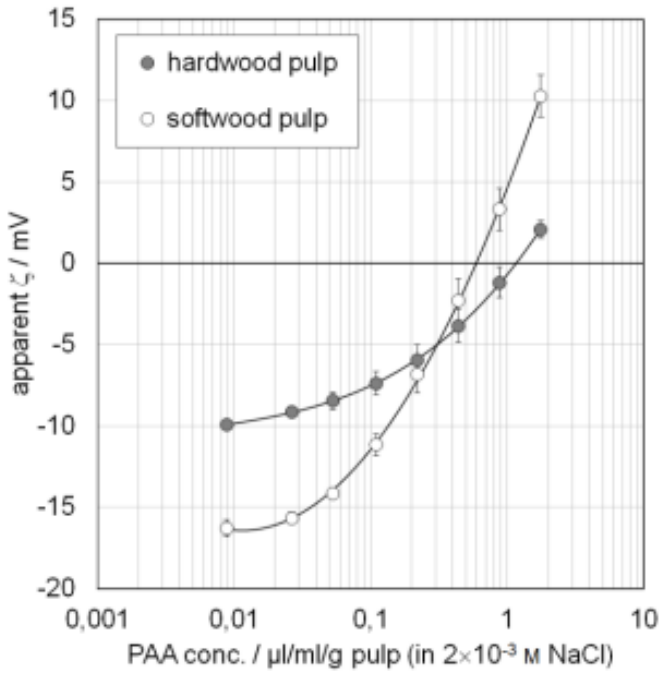

Figure 37: Determination of PZC by titration of pulp with poly(N-acrylamide) at pH 6.9.

The zeta potential provides valuable insights into the surface properties and swelling behavior of lignocellulosic materials. The observed differences between hardwood and softwood highlight their unique interfacial characteristics, influencing compatibility with adhesives and coatings. Higher hydrophilicity and functional group density in hardwoods suggest better bonding potential but also higher susceptibility to swelling, requiring tailored treatments.

The findings also demonstrate the zeta potential's applicability in monitoring chemical modifications and assessing material performance for diverse industrial applications. This technique supports the development of improved wood products and composites by optimizing surface properties and ensuring compatibility with polymers and adhesives.

INSTRUMENTS SUITABLE FOR THESE MEASUREMENTS
SurPASS 3

4.3 APPLICATIONS: COMPOSITE MATERIALS

4.3.1 Determination of suitable testing parameters for DMA testing of composite materials

Advanced composites, such as carbon fiber-reinforced plastics (CFRPs), are critical in structural applications due to their high strength, stiffness, and fatigue resistance at low weight. Understanding their mechanical behavior at varying conditions, particularly the glass transition temperature (Tg), is essential for ensuring performance and reliability. Dynamic mechanical analysis (DMA) in three-point-bending mode is a preferred method for measuring storage modulus (E') and Tg, as it accurately captures the stiffness and viscoelastic behavior of composites, which are often influenced by fiber orientation, surface unevenness, and loading conditions.

The study analyzed unidirectional (CFRP-UD) and twill-weave (CFRP-Fb) carbon fiber-reinforced epoxy composites to evaluate the influence of static force (proportional static force factor, Φ) and displacement amplitude (Δs) on the measured storage modulus.

As can be seen in Figure 38 and Figure 39, at lower Φ values (<600 % for CFRP-UD and <800 % for CFRP-Fb), insufficient static force caused underestimation of stiffness due to poor contact and stress transfer. Higher Φ values stabilized E', with CFRP-UD reaching 126.8 GPa and CFRP-Fb 38.2 GPa. These values aligned with tensile modulus data, considering differences in stress distribution between tensile and bending tests.

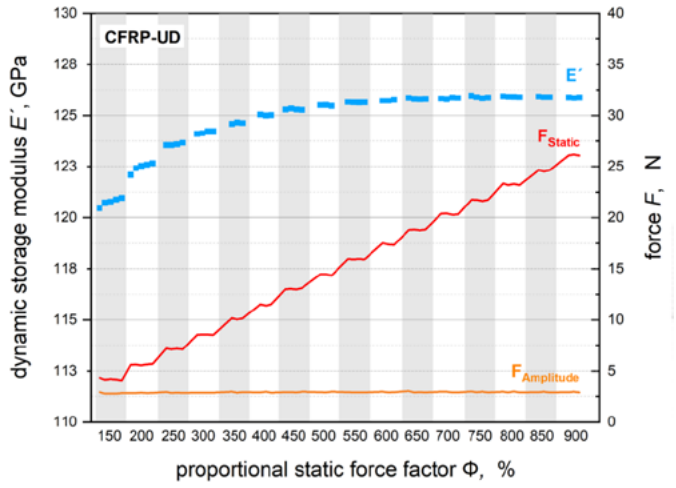

Figure 38: DMA of CFRP-UD in three-point-bending mode at a constant displacement amplitude of 20 µm and increasing proportional static force factor Φ.

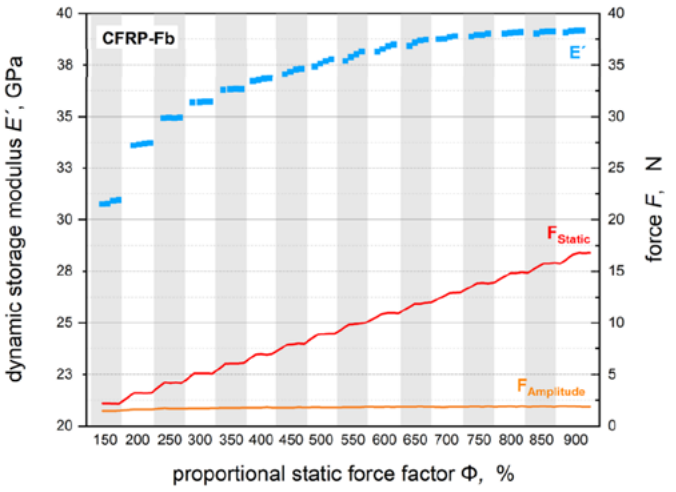

Figure 39: DMA of CFRP-Fb in three-point-bending mode with a constant displacement amplitude of 20 µm and increasing proportional static force factor Φ.

Displacement amplitude (Figures 40 and 41): As illustrated in Figure 40 and Figure 41, increasing Δs revealed a stable range for reliable E' measurements (20 µm to 30 µm) for both materials. Below this range, measurements were less consistent due to insufficient loading. At higher amplitudes, nonlinear viscoelastic effects caused E' to decrease, emphasizing the need to stay within the optimal range.

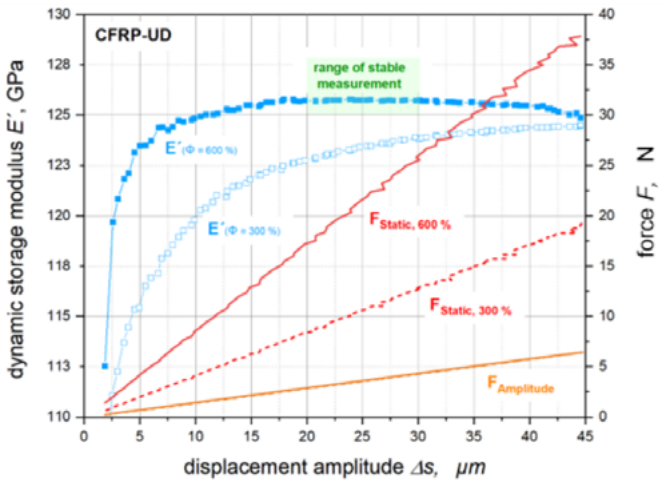

Figure 40: DMA of CFRP-UD in three-point-bending mode with constant proportional force factors and increasing displacement amplitude.

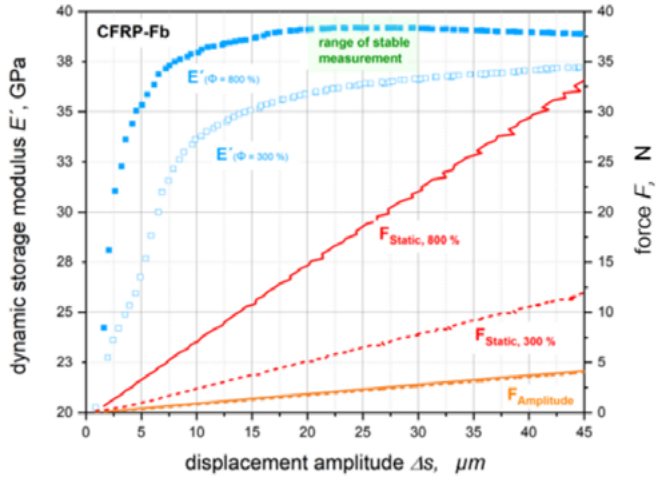

Figure 41: DMA of CFRP-Fb in three-point-bending mode with constant proportional force factors and increasing displacement amplitude.

These results underscore the importance of setting appropriate test parameters in DMA for accurate characterization of composites. Sufficient static force ensures proper specimen contact and stress transfer, critical for materials with uneven surfaces or fiber reinforcement. Determining an optimal displacement amplitude avoids inaccuracies from low stress or nonlinear effects.

The findings also highlight how different fiber orientations influence mechanical responses under bending. CFRP-UD exhibited higher stiffness due to unidirectional reinforcement, whereas CFRP-Fb's lower modulus reflected the influence of woven structure. These results validate DMA as a robust method for assessing viscoelastic properties and guiding the development of high-performance composites for demanding structural applications.

INSTRUMENTS SUITABLE FOR THESE MEASUREMENTS

MCR 702e MultiDrive

4.3.2 Efficient creep investigation of wood-plastic composites in bending mode

Wood-plastic composites (WPCs) are widely used in structural applications, where they endure long-term static loads. Understanding creep behavior – the time-dependent deformation under stress – is critical to ensure material reliability, safety, and longevity. The performance of WPCs depends significantly on the fiber-matrix interface, with poor bonding leading to premature failure. Accurate creep characterization helps optimize composite formulations and predict performance under real-world conditions, guiding material selection and structural design.

Creep tests in three-point bending mode were conducted on pure polypropylene (PP), unmodified fiber-reinforced WPC (PP40/BF60), and fiber-modified WPC (PP40/BFmod60). The deflection curves in Figure 42 highlight differences in deformation and recovery behavior among the materials.

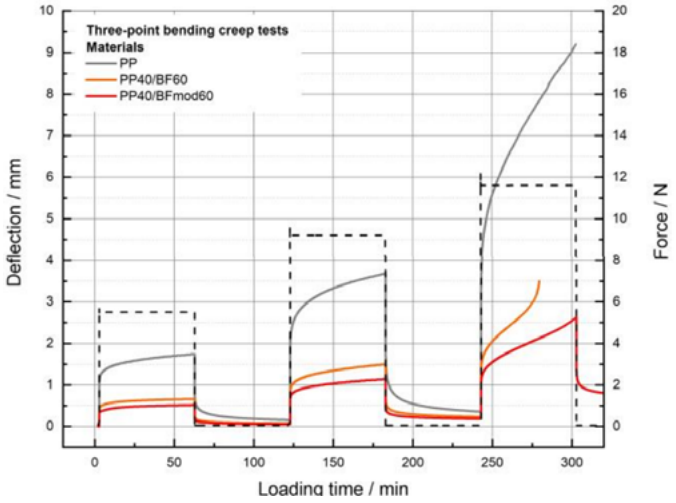

Figure 42: Comparison of the time-dependent deflection behavior of WPC materials under flexural creep loading.

Pure PP showed the largest deformation during loading, reflecting its high viscoelasticity. Creep deformation was pronounced, demonstrating limited suitability for load-bearing applications without reinforcement.

Reinforcement with unmodified fibers significantly reduced deformation compared to pure PP. However, poor fiber-matrix bonding resulted in premature failure at the highest load level, limiting its applicability for high-stress conditions.

The introduction of a coupling agent improved the fiber-matrix interface, further reducing creep deformation and enhancing load capacity. The modified WPC demonstrated superior long-term stability and resilience under increasing loads.

The results demonstrate the importance of fiber-matrix interaction in determining WPC performance. Modified WPC showed reduced creep deformation and higher structural integrity, emphasizing the role of coupling agents in enhancing fiber bonding. The time-dependent deflection curves offer insights into the material's response to prolonged loading and recovery, providing a reliable basis for material qualification.

These findings underscore the need for precise creep characterization to assess material suitability for structural applications. Such testing not only identifies the limitations of unmodified WPCs but also validates the effectiveness of enhancements like fiber modification. This knowledge aids in the development of WPCs with improved durability, making them a sustainable alternative for load-bearing applications.

INSTRUMENTS SUITABLE FOR THESE MEASUREMENTS
MCR 702e MultiDrive

4.4 ARCHITECTURAL FINISHES

4.4.1 Rheological characterization of architectural coatings

Architectural coatings must meet diverse performance criteria at every stage, from liquid application to cured film. Rheological measurements assess critical parameters such as flow behavior, thixotropy, drying speed, and mechanical properties. These insights guide formulation adjustments to improve processability, durability, and visual appeal, ensuring coatings perform effectively under specific application and environmental conditions.

Both wood and metal coatings exhibited shear-thinning behavior, with viscosity decreasing as shear rate increased. At low shear rates, the metal coating showed higher viscosity, but at high shear rates, both coatings converged to similar viscosities. This indicates differing application behaviors, with wood coatings suited for high-shear applications like spraying (Figure 43).

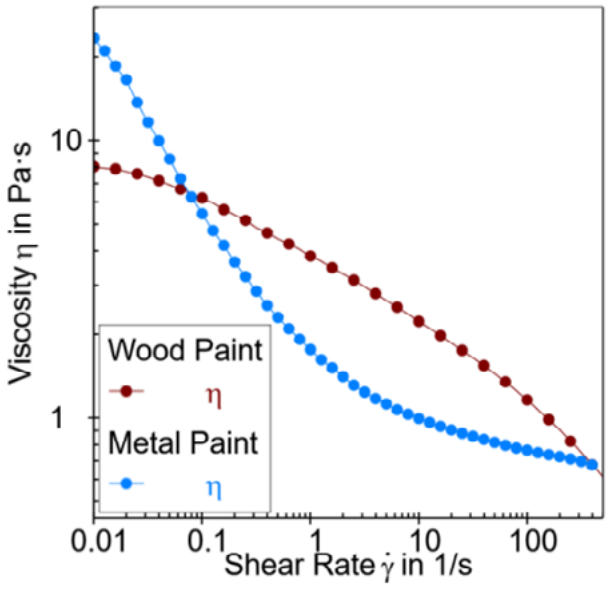

Figure 43: Viscosity curves with shear rates from 0.01 s^{-1} to 500 s^{-1} at 25 °C.

Amplitude and frequency sweeps revealed that wood coating had a broader linear-viscoelastic range (~1.0 % shear strain) compared to the metal coating (~0.5 %). In frequency tests, the wood coating displayed dominant viscous behavior (G" > G') across all frequencies, indicating a tendency for sedimentation over time. The metal coating showed gel-like characteristics (G' > G" at low frequencies), suggesting better sedimentation stability (Figure 44 and Figure 45).

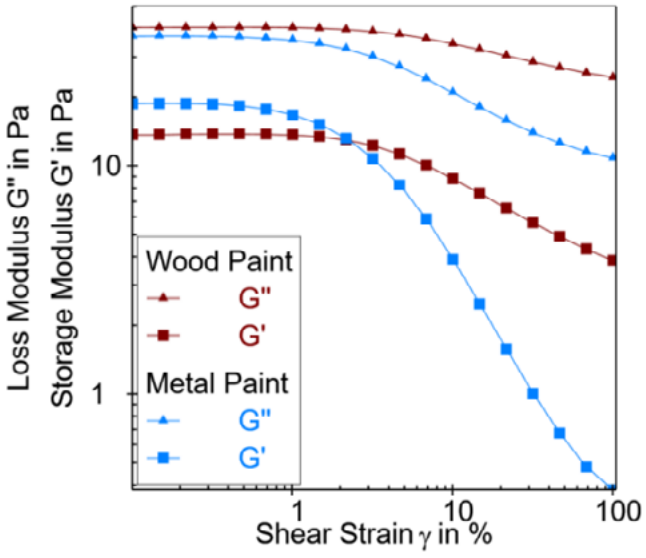

Figure 44: Amplitude tests, measured in the deformation range from 0.1 % to 100 % at the angular frequency of 10 rad/s at 25 °C.

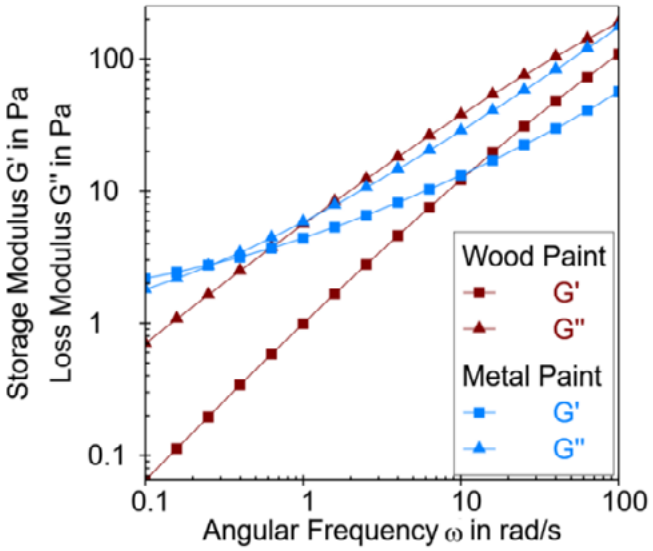

Figure 45: Frequency tests, measured at a deformation of 0.1 % and an angular frequency range of 100 rad/s to 0.1 rad/s at 25 °C.

A 3-Interval Thixotropy Test (Figure 46) showed the wood coating rapidly recovered its structure within seconds after shear, while the metal coating did not fully regenerate even after several minutes. This suggests the wood coating resists sagging and maintains its integrity during application better than the metal coating.

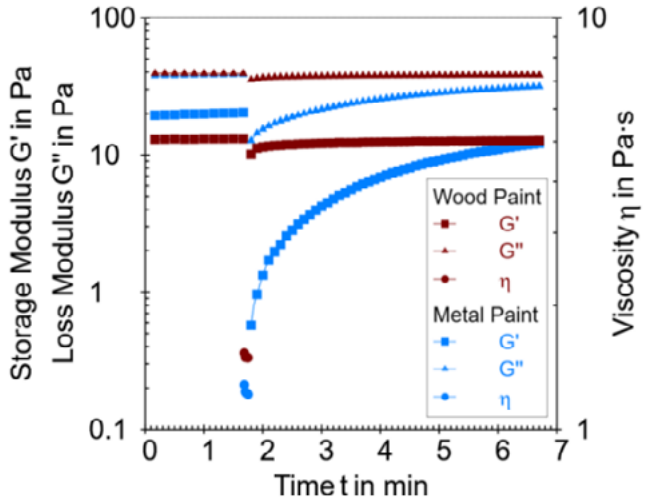

Figure 46: 3ITT measurements, performed at 25 °C.

As can be seen in Figure 47 and Figure 48, humidity significantly impacted drying speed. At 80 % relative humidity, the wood coating transitioned to a viscoelastic solid within ~5 minutes, while the metal coating remained a viscoelastic liquid after 60 minutes. Both coatings showed incomplete curing within this time frame.

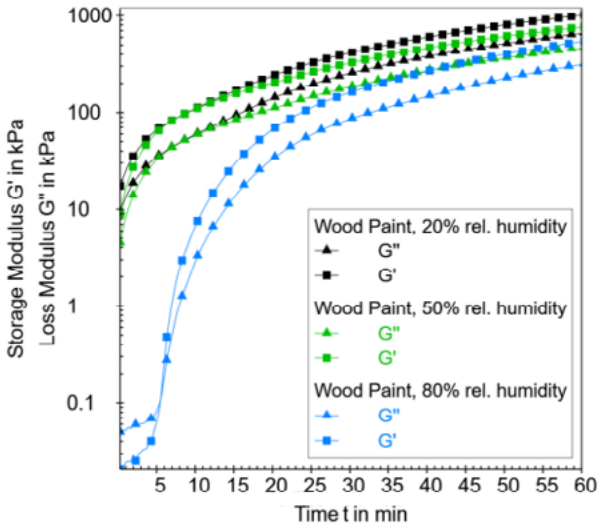

Figure 47: Drying measurements of wood coating at different values of relative humidity at 25 °C.

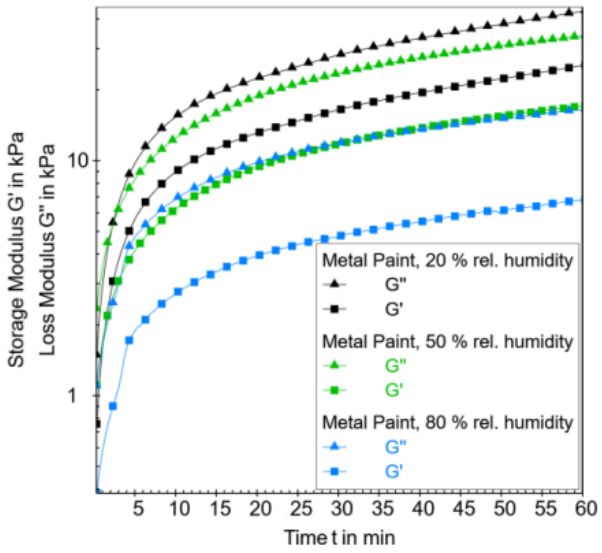

Figure 48: Drying measurements of the metal coating at different values of relative humidity at 25 °C.

As illustrated in Figure 49, tensile tests on the wood coating demonstrated high elasticity, with elongation at break of 16.5 %. This flexibility ensures the coating accommodates wood expansion due to humidity changes without cracking. The metal coating, in contrast, exhibited brittle behavior, indicating potential splintering under substrate movement.

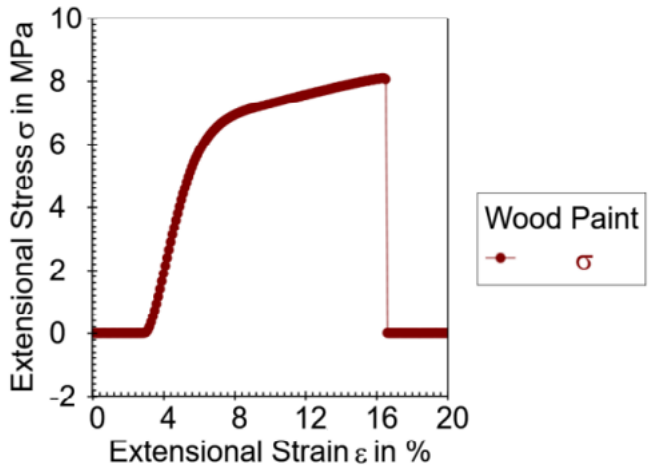

Figure 49: UXF measurement of wood coating with constant strain rate of 0.5 %/s at 25 °C.

These findings highlight distinct performance characteristics of the wood and metal coatings. The wood coating offers rapid structural recovery, better drying speed, and high elasticity, making it suitable for dynamic substrates like wood. The metal coating, with higher sedimentation stability and slower drying, may require process adjustments to improve performance.

Rheological characterization provides a comprehensive understanding of coating behavior, enabling targeted optimization to meet specific application requirements, enhancing durability, and ensuring consistent quality.

INSTRUMENTS SUITABLE FOR THESE MEASUREMENTS
MCR Evolution Series

4.4.2 Viscosity testing of resin-based plasters

The rheological properties of plasters are critical for ensuring their effective application, handling, and performance. Resin-based plasters are used in various construction applications, such as smoothing interior or exterior surfaces and rendering buildings. Measuring their viscosity and flow behavior helps evaluate pumpability, sprayability, and leveling efficiency, ensuring optimal performance during application and achieving the desired finish.

Rheological measurements (Figure 50) revealed that all tested plasters (A, B, and C) exhibit shear-thinning behavior, where viscosity decreases with increasing shear rate. This characteristic enhances their workability during application processes such as spraying and smoothing.

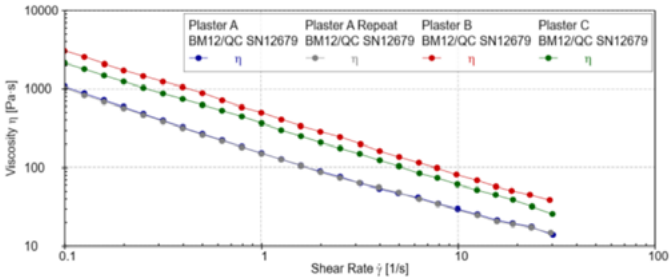

Figure 50: Viscosity curve of three plasters.

Plaster A showed the lowest viscosity values across all tested shear rates, providing better pumpability, sprayability, and faster material flow.

Plasters B and C exhibited higher viscosity values, indicating more resistance to flow but potentially better stability during application.

At a low shear rate of 0.3 s^{-1}, Plaster A had a viscosity of 400 Pa·s, significantly lower than Plaster B (1,240 Pa·s). At higher shear rates (30 s^{-1}), viscosity values converged, with Plaster A at 14 Pa·s and Plaster B at 38 Pa·s, demonstrating their similar flow behavior under higher stress (Table 16).

SHEAR RATE	VISCOSITY PLASTER A	VISCOSITY PLASTER B
0.3 s^{-1}	400 Pa·s	1,240 Pa·s
3 s^{-1}	63 Pa·s	200 Pa·s
30 s^{-1}	14 Pa·s	38 Pa·s

Table 16: Shear rate-dependent viscosities of Plaster A and B.

The shear-thinning behavior of resin-based plasters indicates their suitability for efficient application processes, such as spraying and leveling, where material flow under stress is crucial. The lower viscosity of Plaster A suggests it is more suitable for applications requiring high pumpability and ease of spreading. In contrast, the higher viscosity of Plasters B and C may provide greater stability, reducing sagging during application on vertical surfaces.

By understanding the rheological properties of these materials, manufacturers can optimize formulations to balance workability, stability, and performance, ensuring high-quality finishes for diverse construction applications. Rheological analysis offers a reliable method for comparing and adjusting plaster properties, improving efficiency and consistency in application processes.

INSTRUMENTS SUITABLE FOR THESE MEASUREMENTS
RheolabQC

4.4.3 Characterization of the scratch resistance of ceramic tiles

Ceramic tiles are widely used in flooring applications where they endure wear and scratching from hard objects such as sand or metals. Scratches can reduce their wear resistance, increase surface roughness, and degrade aesthetic qualities like brightness and color. Measuring scratch resistance helps manufacturers ensure tile durability, develop more resistant glazes, and verify quality for specific applications. Since the EN 101 standard for scratch testing is no longer valid, the scratch method offers a robust alternative for evaluating tile performance.

Scratch tests on glazed ceramic tiles identified two critical loads:

→ Lc1: The load at which circular Hertzian cracks appear.

→ Lc2: The load causing brittle fracture (spallation and chipping) of the glaze.

Sample B demonstrated higher Lc1 and Lc2 values compared to Sample A, indicating better scratch resistance. Higher critical loads mean Sample B's glaze resists cracking and brittle failure under greater stresses (Figure 51).

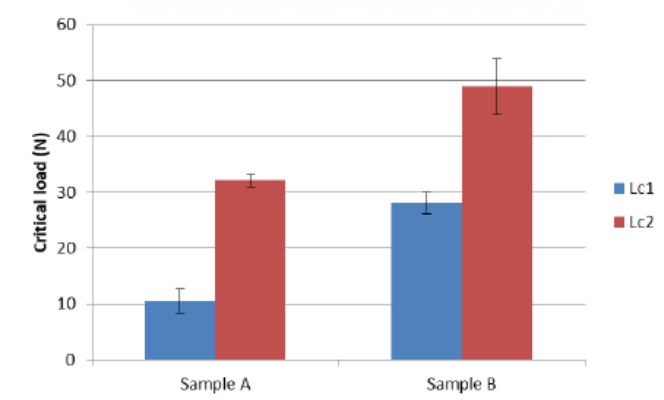

Figure 51: Comparison of critical values for the two types of ceramic tiles with glaze.

Residual depth (Rd) and penetration depth (Pd) were measured to evaluate resistance to permanent deformation (Figure 52 and Figure 53). Sample B showed lower Rd and Pd values, reflecting its superior ability to resist deep scratches and permanent damage. In contrast, Sample A exhibited earlier increases in Rd, correlating with weaker scratch resistance.

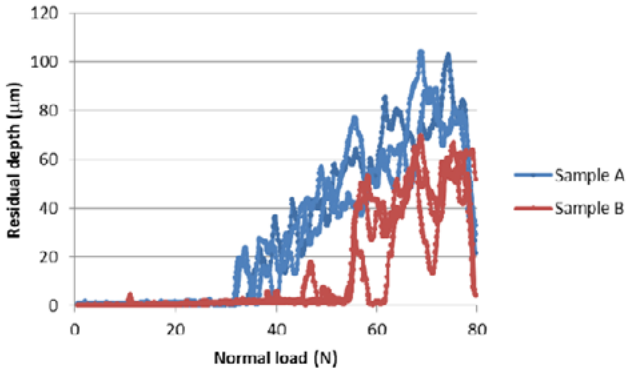

Figure 52: Comparison of residual depth (Rd) signals for Sample A and Sample B (three repetitions for each sample are shown).

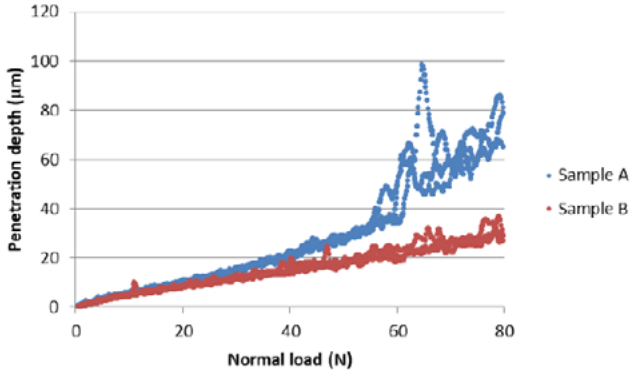

Figure 53: Penetration depth (Pd) curves for samples A and B.

Optical observations provided detailed images of the scratch tracks (Figure 54). Sample B's scratches showed delayed onset of brittle fracture (higher Lc2), confirming its better performance. Panorama images allow quick comparison of failure mechanisms, supplementing critical load measurements.

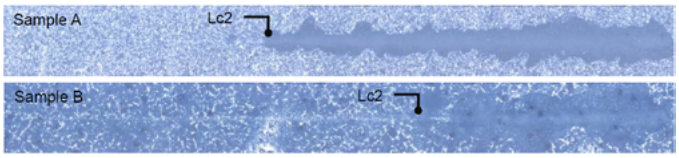

Figure 54: Panorama image of the scratch on Sample A and B with marked Lc2 area.

The results highlight significant differences in the scratch resistance of ceramic tiles with different glazes. Sample B's higher critical loads and lower depth values indicate it is better suited for high-wear environments, offering greater durability and surface integrity. In contrast, Sample A's lower resistance suggests it may perform better in less demanding applications.

These findings demonstrate the utility of scratch testing for assessing ceramic tile quality and aiding in the development of more durable products. By combining mechanical data with visual insights from scratch tracks, this method provides a comprehensive evaluation of material performance, helping manufacturers optimize tile designs for specific use cases.

INSTRUMENTS SUITABLE FOR THESE MEASUREMENTS
RST Series

5 Anton Paar Solutions

MCR Evolution rheometer series
The MCR Evolution series is the result of consistent thinking and rethinking, of continuous development based on decades of experience, and of the feedback of more than 10,000 satisfied customers. The combination of innovative and thousand-fold field-proven technology with the modular design represents the benchmark in its class. With 200+ accessories, the MCR Evolution rheometer series gives you endless possibilities for rheological investigations and material characterization.

Find out more:
www.anton-paar.com/eb-bm-mcr

MCR 702 Multidrive rheometer
The MCR 702e MultiDrive is the most versatile rheometer available. Alongside all standard rheological test modes, it can be equipped with an additional lower drive unit. This means you can perform rheological tests with two torque transducers and drive units at once – opening up multiple possibilities for your research. There are no limitations regarding test modes, measuring systems, accessories, and temperature devices, and no limitations on measurement precision.

Find out more:
www.anton-paar.com/eb-bm-mcr702e

Powder shear and flow cell
The two cells for true powder rheology help you to really characterize and understand your powders. The powder shear cell is ideal for determining the flow behavior of consolidated powders and their time-dependent behavior. Additional accessories provide full control over temperature and humidity. The powder flow cell is an innovative and scientific approach to powder characterization, offering a wide range of test methods.

Find out more:
www.anton-paar.com/eb-bm-cell

FRS Series
Materials which are in regular use in everyday life, such as glasses, ceramics, and metals, are processed or refined as melts at temperatures above 1,000 °C. By determining the melt viscosity of these materials, you can achieve a consistent high quality of the final product and optimize the production process. The Furnace Rheometer Systems (FRS) each combine a highly accurate air-bearing rheometer head and a lab furnace for high-temperature viscosity measurements of melts at furnace temperatures up to 1,800 °C.

Find out more:
www.anton-paar.com/eb-bm-frd

RheolabQC
RheolabQC is a rotational rheometer based on state-of-the-art technologies also used in R&D rheometers. From quick single-point checks and flow curve and yield point determinations, to complex rheological investigations, RheolabQC sets new standards for carrying out routine rheological tests. This powerful rheometer is an excellent example of a modern measuring instrument utilizing all available technical possibilities to ensure flexible, reliable and simple operation.

Find out more:
www.anton-paar.com/eb-bm-rheolabqc

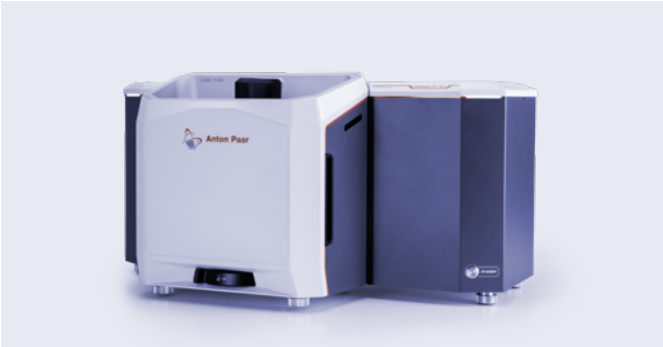

Litesizer DIF 500
With the laser diffraction technology of the Litesizer DIF Series, the particle size and particle size distribution of both liquid dispersions and dry powders from the nanometer up to the millimeter range can be determined. This knowledge is essential for product development and quality control, as these two parameters impact processability as well as the properties of the final product.

Find out more:
www.anton-paar.com/eb-bm-litesizer-dif

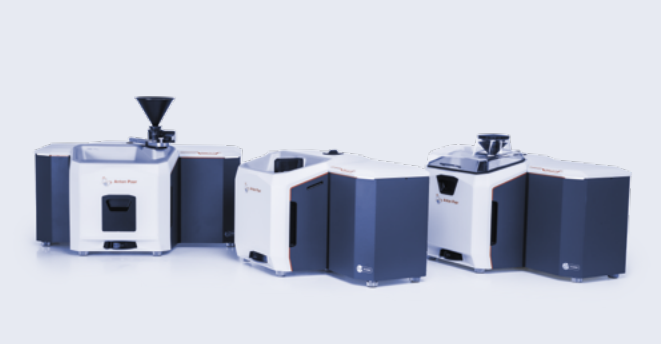

Litesizer DIA Series
With the Litesizer DIA Series, our dynamic image analyzers, you can characterize the size and shape of particles via analysis of their direct images. In just one step, quickly switch among three modules that use dispersion liquid, compressed air, or free-fall and access excellent dispersion of your sample. Rely on automated features, such as feeding rate adjustment and rinsing of liquids, and conduct measurements with only minimal training.

Find out more:
www.anton-paar.com/eb-bm-litesizer-dia

Ultrapyc Series
Ultrapyc gas pycnometers measure the true and skeletal density of solids to track their purity and porosity. Measurements take less than 10 minutes, so they are perfect to control the quality of your solid materials throughout the manufacturing process. The PowderProtect mode enables measurements of fine powders without instrument contamination and the built-in Peltier temperature control ensures superior thermal stability with no external temperature control bath required.

Find out more:
www.anton-paar.com/eb-bm-ultrapyc

Brabender MT-CA
The Brabender MT-CA moisture analyzer, using automated oven drying, measures raw material moisture in a measuring range of >0.1 % and up to 99.9 % moisture content. It reduces test times by 65 % and avoids weighing errors by eliminating the cooling step in the desiccator and automatic back-weighing after drying. It's the perfect choice for moisture determination of powders like flour, tobacco, and solid items with predefined methods that meet international standards.

Find out more:
www.anton-paar.com/eb-bm-mt-ca

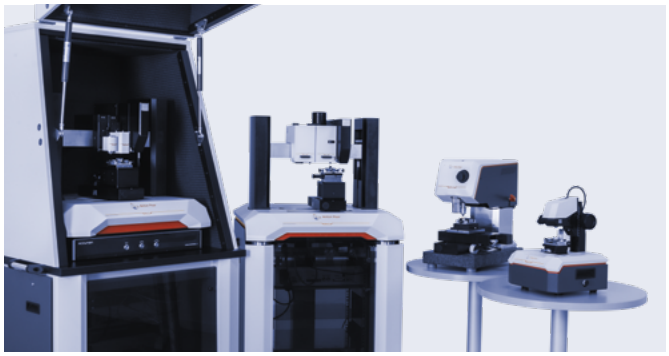

Step platform
Step platforms are the basis for Anton Paar's mechanical surface measuring heads and are the most versatile on the market. With these platforms you can conduct up to four testing methods on a single platform: scratch, indentation, Vickers hardness, and basic tribology. Take advantage of the improved sample navigation features while retaining the high positioning accuracy (<1 µm) over a great length. Customized synthetic granite ensures enhanced vibration damping.

Find out more:
www.anton-paar.com/eb-bm-step

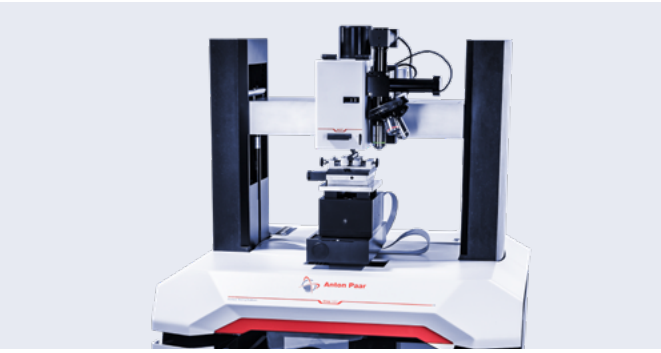

MCT³
The Micro Combi Tester (MCT³) is a universal measurement head for full mechanical characterization of coatings and bulk samples. The unique wide load range of this instrument allows the determination of adhesion, scratch resistance, hardness, elastic modulus, friction, and wear for a wide range of samples. It is applicable to organic and inorganic, as well as soft and hard, coatings (between 1 µm and 20 µm), and also bulk materials.

Find out more:
www.anton-paar.com/eb-bm-mct3

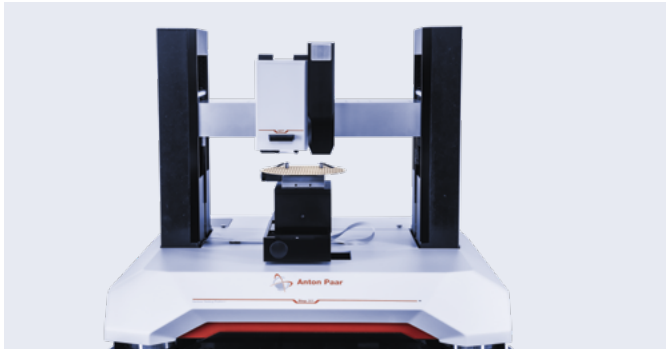

NST³
The Nano Scratch Tester (NST³) is particularly suited for characterizing the scratch resistance and adhesion of thin films and coatings with a typical thickness below 1,000 nm. Analyze organic and inorganic, as well as soft and hard coatings. The unique design of the nano-scratch measurement head includes two sensors for force and depth measurements associated with a state-of-the-art piezoelectric actuator – get results in milliseconds, plus great accuracy and great flexibility.

Find out more:
www.anton-paar.com/eb-bm-nst3

SurPASS 3
The SurPASS 3 Series features fully automated zeta potential analysis of macroscopic solids under real-life conditions. As electrokinetic analyzers, they employ the classic streaming potential and streaming current method for a direct analysis of the surface zeta potential. The zeta potential is related to the surface charge at a solid/liquid interface and is a key parameter for understanding surface properties and developing new specialized materials.

Find out more:
www.anton-paar.com/eb-bm-surpass3

Multiwave 7101, 7301 and 7501
The Multiwave 7101/7301/7501 Series delivers the next level of sample digestion performance and convenience, working at up to 300 °C and up to 199 bar. This ensures complete digestions of all kinds of samples, such as chemicals and metals, but also food, geological, environmental, polymer, cosmetic, pharmaceutical, and petrochemical samples, even in the same run. With a range of accessories, consumables, and racks of up to 28 positions, sample preparation has never been easier.

Find out more:
www.anton-paar.com/eb-bm-multiwave

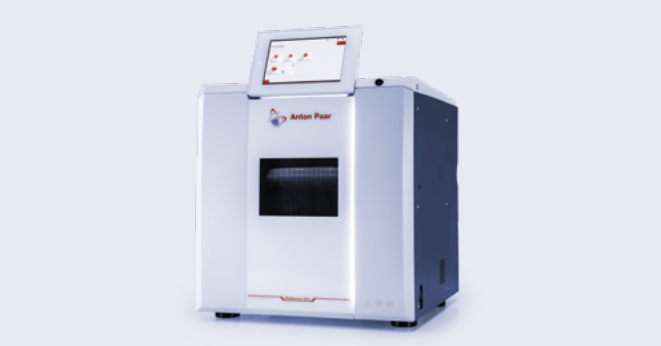

Multiwave 5001
This microwave digestion platform provides digestion of a broad array of samples (varying in difficulty or volume), acid leaching, solvent extraction, evaporation, microwave-induced O_2 combustion, sample drying, and synthesis. Furthermore, it comes with a comprehensive, interactive method library, a customizable, intuitive user interface, and modern sensor technology, together with compact rotors.

Find out more:
www.anton-paar.com/eb-bm-multiwave5001

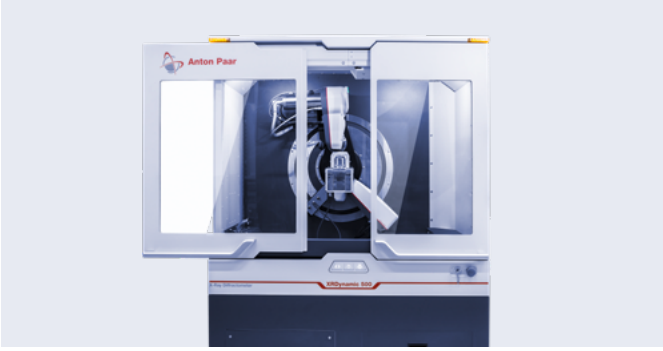

XRDynamic 500
This automated multipurpose powder X-ray diffractometer drives unbeatable XRD data quality with maximum efficiency. It is a versatile platform covering a wide variety of applications with optimal solutions for powder XRD, non-ambient XRD, PDF analysis, SAXS, and more. Intuitive to use, with fully automated optics and alignment routines, it allows everyone, from novices to experts, to collect top-quality XRD data quickly while minimizing errors.

Find out more:
www.anton-paar.com/eb-bm-xrdynamic500

RST series

The Revetest® scratch tester series is the industrial standard, widely used for characterizing hard-coated materials with a typical coating thickness exceeding 1 µm. The RST series includes dependable instruments for the characterization of coating/substrate adhesion, surface scratch resistance, and conventional Vickers hardness.

Find out more:
www.anton-paar.com/eb-bm-rst

References

[1] Hewlet P.C. (1988). Lea's Chemistry of Cement and Concrete. Elsevier Butterworth-Heinemann Publishing, Oxford, UK.

[2] Taylor H.F.W. (1997). Cement Chemistry. Thomas Telford Publishing, London, UK.

[3] Bentz D.P., E.J. Garboczi, C.J. Haecker & O.M. Jensen (1999). Effects of cement particle size distribution on performance properties of Portland cement-based materials. Cement and Concrete Research 29:1663-1671.

[4] Harvey,A. (1998). NIST Interagency/Internal Report No. 5078, pp. 5–7. National Institute of Standards and Technology, Gaithersburg, MD, USA.

[5] Matsui, K., Kikuma, J., Tsunashima, M., Ishikawa, T., Matsuno, S., Ogawa, A. & Sato, M. (2011). Cem. Concr. Res. 41, 510–519.

© 2025 Anton Paar GmbH | All rights reserved.
Specifications subject to change without notice.
XPAIA161EN-A

www.anton-paar.com